Tunneling transport in NSN Majorana junctions across the topological quantum phase transition

New Journal of Physics

The open access journal at the forefront of physics

CrossMark

PAPER

Tunneling transport in NSN Majorana junctions across the topological quantum phase transition

Alejandro M Lobos[1,2] and S Das Sarma[2]

1   Facultad de Ciencias Exactas Ingeniería y Agrimensura, Universidad Nacional de Rosario and Instituto de Física Rosario, Bv. 27 de Febrero 210 bis, 2000 Rosario, Argentina

2   Condensed Matter Theory Center and Joint Quantum Institute, Department of Physics, University of Maryland, College Park, MD 20742-4111, USA

E-mail: lobos@ifir-conicet.gov.ar

Abstract

We theoretically consider transport properties of a normal metal (N)-superconducting semiconductor nanowire (S)-normal metal (N) structure (NSN) in the context of the possible existence of Majorana bound states in semiconductor–superconductor hybrid systems with spin–orbit coupling and external magnetic field. We study in detail the transport signatures of the topological quantum phase transition (TQPT) as well as the existence of the Majorana bound states in the electrical transport properties of the NSN structure. Our treatment includes the realistic non-perturbative effects of disorder, which is detrimental to the topological phase (eventually suppressing the superconducting gap completely), and the effects of the tunneling barriers (or the transparency at the tunneling NS contacts), which affect (and suppress) the zero bias conductance peak associated with the zero-energy Majorana bound states. We show that in the presence of generic disorder and barrier transparency the interpretation of the zero bias peak as being associated with the Majorana bound state is problematic since the non-local correlations between the two NS contacts at two ends may not manifest themselves in the tunneling conductance through the whole NSN structure. We establish that a simple modification of the standard transport measurements using conductance differences (rather than the conductance itself as in a single NS junction) as the measured quantity can allow direct observation of the non-local correlations inherent in the Majorana bound states. We also show that our proposed analysis of transport properties of the NSN junction enables the mapping out of the topological phase diagram (even in the presence of considerable disorder) by precisely detecting the TQPT point. We propose direct experimental studies of NSN junctions (rather than just a single NS junction) in order to establish the existence of Majorana bound states and the topological superconducting phase in semiconductor nanowires of current interest. Throughout the work we emphasize that the NSN transport properties are sensitive to both the bulk topological phase and the end Majorana bound states, and thus the NSN junction is well-suited for studying the non-local correlations between the end Majorana modes as well as the bulk TQPT itself.

1. Introduction

The subject of topological superconductors (SCs) hosting non-Abelian quasiparticles has become one of the most intensively investigated topics in condensed matter physics [1, 2]. In particular, one-dimensional (1D) topological SCs have been predicted to support zero-energy particle–hole symmetric non-Abelian Majorana bound-states (MBS) localized at the ends [2]. Beyond their intrinsic fundamental interest, MBS have attracted attention for their potential use in fault-tolerant topological quantum computation schemes [3]. Far from being a subject of purely theoretical interest, concrete experimental proposals to realize these exotic states of matter have been put forward recently [4–8], some of which have been implemented experimentally [9–14]. In

particular [6–8], showed that a 1D semiconductor nanowire in proximity to a bulk *s*-wave SC, and subjected to strong Rashba spin–orbit coupling can be driven into a topologically non-trivial phase with MBS localized at the ends, upon the application of an external Zeeman magnetic field. In this topologically non-trivial phase, the nanowire becomes *effectively* a helical spinless *p*-wave SC, realizing an idea originally proposed by Kitaev for the localization of isolated MBS in a physical system [2]. Other experimental setups involving arrays of magnetic atoms on *s*-wave SCs [15], or cold-atomic systems [16] have also been proposed and are currently under experimental consideration. It is important to mention here that the real significance of course is the creation of isolated zero-energy MBS at the ends of the nanowire which are well-separated from each other so that they can be considered topologically protected.

On the experimental side, one of the most relevant questions is how to establish the presence of 'true' MBS in a real experiment. In principle, the tunneling conductance at the end of the topological SC nanowire should reveal an MBS as a quantized zero-bias peak (ZBP) of magnitude $2e^2/h$ in the conductance at zero temperature, which is a direct manifestation of the perfect Andreev reflection associated with the MBS [8, 17–21]. Recent experiments implementing the proposal in [6–8] have shown an intriguing ZBP, in apparent agreement with theoretical predictions for the existence of MBS, which appears upon application of a Zeeman field, providing compelling preliminary evidence of the Majorana scenario [9–11]. However, the interpretation of these experiments seems to be considerably more complex than the ideal models originally proposed and show several deviations from the predicted behavior, among which we mention the most important ones: (a) the smallness of the ZBP in comparison to the ideally theoretical value of $2e^2/h$ (i.e., $0.1-0.2$ e^2/h in the low temperature limit), (b) the presence of a continuum of fermionic excitations in the subgap region (i.e., the so-called 'soft-gap' feature) instead of a well-defined SC gap, and (c) the lack of evidence for the closing and then reopening of this SC soft-gap upon increasing the Zeeman field across the putative critical field V_c. We stress that this last feature is a crucial prerequisite for the existence of MBS, which would be indicative of a topological quantum phase transition (TQPT) taking place in the sample where the gap must vanish.

Contrasting with the interpretation that the recent nanowire experimental observations are indeed evidence for the isolated existence of MBS in a topological SC system, it has been pointed out that other ZBPs (or near-ZBPs) sharing similar features with the MBS are generically allowed in spin–orbit-coupled nanowires subject to a magnetic field in the presence of disorder or smooth confining potentials, both in the topologically trivial and non-trivial phases, a fact that would hinder the observation of bona fide Majorana-type excitations [22–26]. In particular, disorder is known to have strong detrimental effects in *p*-wave SCs [27–42]. Motrunich *et al* showed more than a decade ago that Andreev subgap states induced by disorder tend to proliferate in 1D systems described by Bogoliubov–de Gennes Hamiltonians with broken time and spin-rotational symmetry (symmetry class D, like the nanowires in [6–8]), and render the system gapless [27]. These authors predicted that for weak disorder an infinite system realizes a topologically non-trivial phase with two degenerate zero-energy MBS localized at the ends of the wire. In a finite-length system of size L_w, this degeneracy is lifted by an exponential splitting $\Delta\varepsilon \sim e^{-L_w/\xi}$, where ξ is the superconducting coherence length. Increasing the amount of disorder generates low-energy Andreev bound states, and the (averaged) scaling of the splitting energy changes to $\Delta\varepsilon \sim e^{-L_w/\xi + L_w/(2\ell_e)}$, where ℓ_e is the elastic mean-free path of the system [30]. Beyond a critical disorder amount, defined by the condition $\ell_e = \xi/2$, the system experiences a TQPT induced by disorder and enters a non-topological insulating phase with no end-MBS. At both sides of the TQPT, the system is *localized* at zero energy, and exactly at the critical point separating these phases, the wave functions become *delocalized* and the smallest Lyapunov exponent (i.e., the inverse of the localization length of the system) vanishes. This intimate connection between localization and topology in disordered topological SCs has been stressed in a series of theoretical works [27, 33, 34, 39]. The interplay among disorder, superconductivity, and possible Majorana zero modes is still very much an important open problem in the subject, and whether the experimentally observed ZBP is indeed the manifestation of the theoretically predicted MBS can only be sorted out definitively by accurately understanding the precise role of disorder in the experimental systems. In particular, a key question is the effect of disorder on the TQPT itself, which is a central topic of the current work.

Concerning the rather ubiquitous presence of in-gap states (or 'soft gap') in the experiment, it is important to note the lack of evidence of a well-defined superconducting gap in most of the experiments involving evaporated SC-semiconductor SN contacts, even in absence of an applied magnetic field, when the time-reversal symmetry is not broken (i.e., symmetry class DIII or BDI). By improving the quality of the semiconductor/SC interface using molecular beam-epitaxy methods, as was theoretically predicted [43], recent experiments have reported much harder gaps [44, 45], suggesting that some sort of disorder at the might be operative at the SN interface. Since the topological protection of the MBS is directly provided by the existence of the SC gap, it is of obvious importance to understand the physical origin of this soft gap for the correct interpretation of the experiment (as well as to help produce hard gap systems for future Majorana experiments). Stanescu *et al* have suggested recently that intrinsic quasiparticle broadening effects due to the hybridization of the SC with the
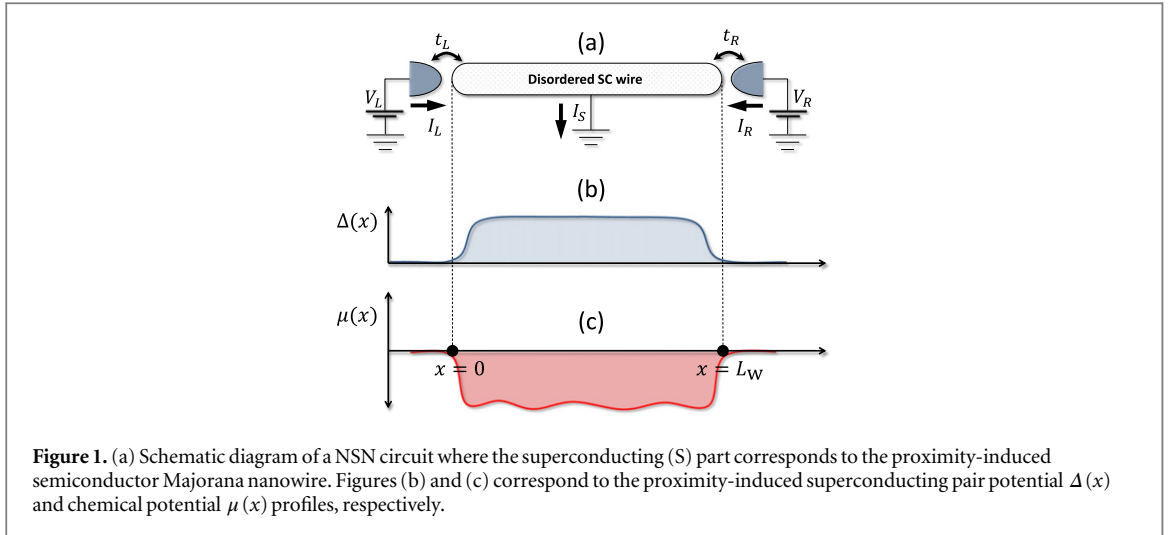
normal metallic lead, could explain this feature [46]. Indeed, it is well-known that a highly transparent NS barrier can produce large subgap conductance [47] (i.e. Blonder–Tinkham–Klapwijk (or BTK) barrier parameter $Z \to 0$), and therefore could also induce a large broadening of Bogoliubov quasiparticles, and hence a soft gap through this 'inverse proximity effect' of the normal metallic lead on the SC nanowire. However, this does not seem to be the complete explanation of the experiment. Recent experiments where the transparency of the NS contact was systematically reduced have shown that the soft gap persists even in the low-transparency limit (i.e., 'pinching off' the quantum point contact when the inverse proximity effect should be exponentially suppressed) [14, 45]. An alternative explanation for the soft gap, valid in the limit of low transparency (i.e., large BTK barrier parameter $Z \to \infty$), was proposed in [43]. Among the many different pair-breaking mechanisms that might be operative in Majorana nanowires as considered in [43] (e.g., finite temperature T, presence of magnetic impurities, quasiparticle broadening, etc) realistic parameter considerations point to the predominance of a special kind of inhomogeneity, which was not considered before in the present context: the spatial fluctuations in the proximity-induced pair potential $\Delta(x)$ [43]. Physically, spatial fluctuations in $\Delta(x)$ are likely to be introduced by disorder or inhomogeneities at the SC/semiconductor contact[3]. Following the suggestion of the theoretical explanation given in [43], the above-mentioned experiments involving epitaxially grown SC/semiconductor nanowires [44, 45] have reported much harder gaps. This constitutes a qualitative improvement in the fabrication of Majorana nanowires, and hopefully a new generation of experiments where disorder effects are dramatically reduced will be soon available with hard proximity gaps (i.e. no subgap fermionic excitations) and well-defined MBS. We incorporate this aspect of the soft gap physics in the current work through a simple model approximation which mimics the spatial variation in the proximity-induced superconducting pair potential arising from the inhomogeneities at the SC-nanowire interface (see equation (4) below and the associated discussion).

The above discussion describes the rather complex situation faced in the experiments in order to detect 'true' MBS in the topological phase. In this article we focus on a specific configuration, the normal-topological superconductor-normal (NSN) configuration, which is currently under experimental study. The SC part of this NSN (i.e. the S-part) junction is the semiconductor nanowire which has proximity-induced superconductivity from an underlying ordinary *s*-wave SC system. Many of the recent experiments have focused specifically on just the simple NS junction, but NSN junctions are essentially 'equally easy' to study, and they have been studied also. We believe that NSN junctions have some intrinsic advantages over the minimal NS junction transport for studying MBS physics and the associated TQPT. We provide a comprehensive theoretical analysis of its transport properties taking into account the effects of disorder, inhomogeneities and temperature. As noted in previous works, the NSN configuration allows to extract the same information as in the simpler NS contacts, but contains additional interesting new physics arising from non-local correlations [48–51].

The current work is a generalization and extension of our earlier work in [39], where we introduced an original proposal for a direct experimental study of the Majorana fermion-related TQPT in hybrid semiconductor nanowire structures. Here, we present a more detailed study of the tunneling transport properties of the NSN junction, a fact that allows us to make contact with recent and ongoing experiments [9–11, 13, 14]. In contrast to our previous [39], where we computed the differential conductance *only* at one end of the NSN system, at zero bias voltage and at zero temperature, in this work we extend our calculation to the *full* differential conductance matrix (see equation (1)) at finite bias voltage. In addition, we also study the thermal effects (see figure 5), which are important in order both to quantify the detrimental effects on the efficiency of our proposed detection scheme for the TQPT (see equation (17)), as well as for allowing a more realistic comparison with the experiments. Finally, in this work we also provide a physically intuitive theoretical description (see section 6) of the proposed experiment in terms of an exaclty solvable 'random-mass' Dirac model, where the interplay between disorder, external magnetic fields, and the emergence or destruction of MBS, is made fully transparent.

While this is not a 'smoking-gun' experiment, it might be an extremely useful experimental tool providing information about the topological phase diagram of the system, complementary to non-local shot noise correlations [48–51]. Observation of non-local correlations as well as studying the TQPT itself using our suggested transport techniques in NSN junctions taken together may in fact serve as the smoking gun evidence for the existence of Majorana modes in nanowire systems. An associated significant advantage of the NSN junctions over the much-studied NS junctions in the context of Majorana physics in nanowires, which should be obvious from the above discussion and is emphasized throughout this work, is that transport in NSN junctions potentially studies both the end MBS and the bulk topological SC phase whereas NS junction tunneling

---

[3] The oxide layer that inevitably forms around the semiconductor nanowires needs to be removed in order to create a good contact with the superconductor, a step which is typically done by ammonium sulfide etching, sometimes followed by Ar plasma etching. The amophous superconducting layer is then deposited on top of the semiconductor by sputtering techniques. While this process is effective in removing the oxide layer in the semiconductor, it inevitably damages the nanowire surface.

Figure 1. (a) Schematic diagram of a NSN circuit where the superconducting (S) part corresponds to the proximity-induced semiconductor Majorana nanowire. Figures (b) and (c) correspond to the proximity-induced superconducting pair potential $\Delta(x)$ and chemical potential $\mu(x)$ profiles, respectively.
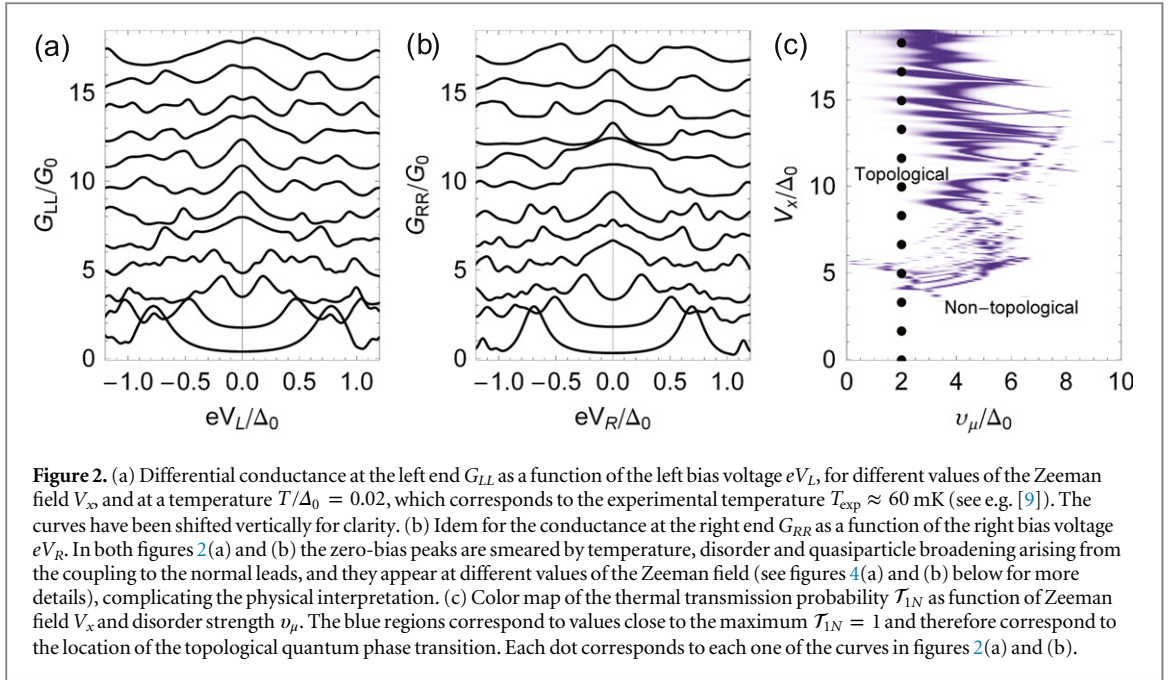
properties may very well be dominated by the end MBS so as to suppress the manifestation of the bulk TQPT and the non-local correlations between the two end MBS which must go through the bulk nanowire. This is the key reason for our promoting NSN junction transport studies as an important tool for the Majorana investigation.

In order to illustrate the main motivation of this article, let us first consider a 'dirty' proximity-induced SC Majorana nanowire, electrically connected to ground and attached to normal contacts in a NSN configuration, as shown schematically in figure 1(a). Here we consider a generic situation where inhomogeneities are present both in the form of spatial fluctuations of the (proximity-induced) pairing potential, and in the form of quenched disorder in the on-site chemical potential fluctuations (figures 1(b) and (c)). We also assume an external Zeeman field applied in the direction parallel to the nanowire, which allows to drive the system across the TQPT. A relevant experimental quantity is the differential conductance matrix, defined as

$$G_{ij}\left(eV_j\right) \equiv \frac{\mathrm{d}I_i}{\mathrm{d}V_j}\left(eV_j\right), \tag{1}$$

where I_i and V_j are, respectively, the current and voltage applied in the $\{i, j\} = \{L, R\}$ normal contact. In ideal conditions, the local conductances G_{LL} and G_{RR} should reveal the presence of end-MBS as a quantized ZBP peak of magnitude $2e^2/h$ at $T = 0$ [8, 17–19]. In practice, however, disorder, finite temperatures, quasiparticle poisoning, etc, might hinder or even destroy the purported topological phases and, therefore, the MBS. Since we are motivated by the current experiments, we start by showing a typical example of our numerical simulations of tunneling transport in figures 2(a) and (b), and leave the explanation of the theoretical details for sections 2–4. In these plots have computed the local conductances G_{LL} and G_{RR} for a disordered wire at a finite temperature as a function of the local bias voltages V_L and V_R, respectively, and for different values of the applied Zeeman field. In contrast to the ideal case [52] (i.e., clean system and $T = 0$), where a vanishing single-particle excitation gap signals the TQPT across the critical Zeeman field, with the ZBP emerging on the topological side at higher magnetic field, here the presence of the above mentioned non-idealities renders the situation much less clear to determine the TQPT and the nature of the ZBPs. In other words, the information about the ZBP has been 'washed out' by a combination of thermal effects, disorder and quasiparticle broadening, although the conductance results in figure 2 are explicitly obtained theoretically in a system where the MBS definitively exists in the ideal situation. (As an aside, we mention that the theoretical conductance results depicted numerically in figure 2 look remarkably similar to the measured tunneling spectroscopy results reported so far in the literature in the context of Majorana nanowire experiments.) The ZBPs emerge in a soft-gap background and, in agreement with recent experimental results, the left and right ZBPs appear and disappear at different values of the Zeeman field (i.e., they appear not to be correlated). Is the wire 'fragmented', so that the end Majoranas do not know about the existence of each other? What is the topological state of the nanowire? Does the wire have more than one pair of MBS because of disorder? How do we establish the existence of MBS using such imperfect ZBP data in a manifestly soft gap situation? These are the kind of questions that motivate our work.

The article is divided as follows. In section 2 we present the theoretical framework, the model and the main approximations. In section 3 we describe the method used to determine theoretically the topological phase diagram of a disordered Majorana wire. In section 4 we present the theoretical technique to describe the differential conductance of a generic disordered Majorana wire in the NSN configuration and analyze the physical content in the analytical expressions. In section 5 we describe in detail a proposal to extract information about the TQPT and to assess the topological stability of MBS. Section 6 is intended to provide a simple intuitive theoretical understanding the physics underlying our proposal, in section 7 we present a summary and our

Figure 2. (a) Differential conductance at the left end G_{LL} as a function of the left bias voltage eV_L, for different values of the Zeeman field V_x, and at a temperature $T/\Delta_0 = 0.02$, which corresponds to the experimental temperature $T_{exp} \approx 60$ mK (see e.g. [9]). The curves have been shifted vertically for clarity. (b) Idem for the conductance at the right end G_{RR} as a function of the right bias voltage eV_R. In both figures 2(a) and (b) the zero-bias peaks are smeared by temperature, disorder and quasiparticle broadening arising from the coupling to the normal leads, and they appear at different values of the Zeeman field (see figures 4(a) and (b) below for more details), complicating the physical interpretation. (c) Color map of the thermal transmission probability $\mathcal{T}_{1N}$ as function of Zeeman field V_x and disorder strength υ_μ. The blue regions correspond to values close to the maximum $\mathcal{T}_{1N} = 1$ and therefore correspond to the location of the topological quantum phase transition. Each dot corresponds to each one of the curves in figures 2(a) and (b).

conclusions, and finally in appendix we give a detailed derivation of the equations (11)–(14) for the conductance matrix in the NSN configuration.

2. Theoretical model

In accordance with previous works on Majorana wires, [6, 7, 52] we consider the following Hamiltonian describing a disordered semiconductor nanowire of length L_w, subjected to Rashba spin–orbit coupling and a Zeeman field, $H_{NW} = H_0 + H_\Delta$, where

$$H_0 = \int_0^{L_w} dx \ \psi_\sigma^\dagger(x) \left[-\frac{\partial_x^2}{2m} - \mu(x) + i\alpha_R \hat{\sigma}_y \partial_x \right. $$
$$\left. + V_x \hat{\sigma}_x \right]_{\sigma\sigma'} \psi_{\sigma'}(x), \tag{2}$$

$$H_\Delta = \int_0^{L_w} dx \ \Delta(x) \left[\psi_\uparrow^\dagger(x)\psi_\downarrow^\dagger(x) + \psi_\downarrow(x)\psi_\uparrow(x) \right]. \tag{3}$$

Here, $\psi_\sigma^\dagger(x)$ creates a fermion with spin projection σ, and $\hat{\sigma}_i$ (with $i = x, y, z$) are the Pauli matrices acting on spin space. The parameter α_R is the Rashba spin–orbit coupling strength and V_x is the Zeeman field along the wire, and summation over repeated indices σ is implied. The term H_Δ represents the effect of a proximate bulk s-wave SC on the nanowire (not shown in figure 1(a)), which induces a mean-field SC pairing potential $\Delta(x)$ through the proximity effect. For simplicity, we have assumed single-channel occupancy in the nanowire with no loss of generality. As we will explain later, our results are generic and this single-channel (or single-subband) assumption does not affect the main conclusions in the case of many occupied subbands (as long as an odd number of subbands are occupied which is a necessary condition for the existence of the MBS for many occupied subbands [53]). We recall that H_{NW} is only an effective 1D model describing the system at low temperatures. A more realistic model should involve an explicit coupling $t_\perp$ to the proximate bulk SC, which is the source of superconducting correlations, and a self-consistent determination of $\Delta(x)$. However, this task is beyond the scope of this work and does not change our results qualitatively since all we need in our model is the existence of a pairing potential in the nanowire. For more details, we refer the reader to [52, 54] where a deeper discussion on this issue is provided, which is not particularly germane for our consideration in the current work where we are interested in the realistic manifestation of the MBS themselves rather the issue of proximity effect.

Disorder and inhomogeneities enter in the above model through two physically different mechanisms: (a) local fluctuations of the chemical potential $\mu(x) = \mu_0 + \delta\mu(x)$, with μ_0 a uniform value which in principle can be controlled by external gates, and the fluctuations $\delta\mu(x)$ are physically related to the presence of impurities, vacancies, etc in the environment (both the nanowire itself and the surrounding). We assume $\delta\mu(x)$ to be a Gaussian random variable fully characterized by $\langle \delta\mu(x) \rangle = 0$ and $\langle \delta\mu(x)\delta\mu(y) \rangle = \upsilon_\mu^2 \delta(x - y)$, with the

standard deviation v_μ representing the 'strength' of disorder (see the horizontal axis in figure 2(c)). For one single realization of disorder, once the nanowire is deposited and electrically contacted, we assume this parameter to be fixed throughout the experiment. (b) Local variations in the (induced) pair potential $\Delta(x)$, which for concreteness (and numerical convenience) here we model as

$$\Delta(x) = \Delta_0 \tanh\left(\frac{x}{d_\Delta}\right) \tanh\left(\frac{L_w - x}{d_\Delta}\right), \tag{4}$$

for $0 < x < L_w$, i.e., a smooth profile that vanishes at the ends of the nanowire. Here Δ_0 is the value in the bulk (i.e., right next or beneath the bulk SC), and d_Δ is an adjustable parameter that controls the slope of the profile. As mentioned above, a more rigorous treatment of this mean-field Hamiltonian should involve a self-consistent determination of this profile, but for our present purposes this simplification is well justified. In contrast to [43], here we only consider the deterministic profile equation (4) and we neglect other random inhomogeneities in $\Delta(x)$ introduced by disorder. More details on disorder-induced SC pairing potential fluctuations can be found in [43].

In the absence of disorder and in the uniform case (i.e., limit $v_\mu = d_\Delta = 0$), the Hamiltonian H in the limit $L_w \to \infty$, can be easily diagonalized in momentum space k. In that case, the dispersion relation for the Bogoliubov quasiparticles is [5, 7] $E_{k,\pm}^2 = V_x^2 + \Delta_0^2 + \xi_k^2 + \left(\alpha_R k\right)^2 \pm 2\sqrt{V_x^2 \Delta_0^2 + \xi_k^2 [V_x^2 + (\alpha_R k)^2]}$, with $\xi_k = \hbar^2 k^2 / (2m) - \mu_0$. For given values μ_0, Δ_0 and α_R, this model has a TQPT as a function of magnetic field V_x (i.e., the Zeeman spin splitting) from a topologically trivial phase to a non-trivial phase with the appearance of MBS localized at the ends of the nanowire at the critical Zeeman field value $V_{x,c} = \sqrt{\Delta_0^2 + \mu_0^2}$, as originally shown by Sau *et al* [5]. In the presence of disorder and other spatial fluctuations of the parameters in the model, the critical field $V_{x,c}$ typically shifts to larger values and its value depends on the precise details of the disorder realization [31, 34, 35, 38, 39]. The determination of the critical field defining the TQPT is then non-trivial and has to be done numerically for a given disorder realization. This is the subject of the next section.

Finally, we mention that our NSN system is actually conceptually (and perhaps practically too) simpler than the usual NSN system (where the 'S' part is an intrinsic SC) because of the proximate nature of the superconductivity induced in the nanowire from the metallic SC underneath the semiconductor. Thus various complications (e.g. dissipation, cooling, self-consistency, nontrivial Fermi distribution, electron heating, etc) which might make the description of the usual NSN structures difficult [55] are most likely irrelevant in our system, where the 'S' part is the nanowire on a real SC, making our theoretical description easier than that for the standard NSN structures with 'S' being a real superconducting nanowire connected to two normal metallic tunnel contacts.

3. Thermal transport and topological phase diagram of a dirty Majorana nanowire

Let us now focus on the topological phase diagram of the disordered Majorana nanowire. In order to make progress, we have discretized the Hamiltonian in equations (2) and (3), and obtained a N-site tight-binding model with the lattice parameter a (see [52])

$$
\begin{aligned}
H_{NW} = &-t \sum_{\langle lm\rangle,\sigma} c_{l,\sigma}^\dagger c_{m,\sigma} - \sum_{l,\sigma} c_{l,\sigma}^\dagger \left(\mu_l - V_x \hat{\sigma}_{\sigma\sigma'}^x\right) c_{l,\sigma'} \\
&+ \sum_{l,\sigma} \left(i\alpha\, c_{l,\sigma}^\dagger \hat{\sigma}_{\sigma\sigma'}^y c_{l+1,\sigma'} + \Delta_l c_{l\uparrow}^\dagger c_{l\downarrow}^\dagger + \text{h.c.}\right),
\end{aligned}
\tag{5}
$$

where $c_{l,s}^\dagger$, μ_l and Δ_l are the discrete versions of $\psi_\sigma^\dagger(x)$, $\mu(x)$ and $\Delta(x)$, respectively, and $t = \hbar^2/2m_e a^2$ is the effective hopping parameter. Here $\alpha = \sqrt{m\alpha_R^2/2}$ is the corresponding Rashba coupling parameter in the tight-binding model. The first site at the left end corresponds to $l = 1$ and the final site at the right is $l = N$.

We consider a *single* distribution of μ_l (disorder realization), and systematically vary its dispersion v_μ around the mean value μ_0. As mentioned above, v_μ is not an experimentally tunable parameter, but it is useful and instructive to visualize the topological phase diagram as a function of varying disorder. Presumably, a fixed disorder realization is closer to the experiment, where the semiconductor nanowire is in the mesoscopic regime, and it is not clear that disorder necessarily self-averages at the very low experimental temperatures. We mention that whether the experimental temperatures are low enough so that the system is not self-averaging (so that mesoscopic fluctuations are important as one goes from one sample) is currently not known for the Majorana experiments, and the issue of whether to ensemble average over disorder realizations or not for quantitative comparison with experiments remains open at this stage.

We compute the topological phase diagram of the *isolated* nanowire (i.e., in absence of the normal contacts) using the transfer-matrix approach [34, 39] for the model Hamiltonian equation (5), as a function of the disorder strength v_μ and the external Zeeman field V_x. Physically, the transfer matrix relates states in the left end

to states in the right end of the wire. This statement can be made more precise introducing the Majorana basis $c_{l,\sigma} = \left(a_{\sigma,l} + i b_{\sigma,l} \right) \big/ \sqrt{2}$, where the Majorana operators obey the anti-commutation relations $\{ a_{\sigma,l}, a_{s,m} \} = \left\{ b_{\sigma,l}, b_{s,m} \right\} = \delta_{l,m} \delta_{\sigma,s}$ and zero otherwise. In terms of these operators, a generic eigenmode Ψ of H_{NW} satisfying the eigenvalue equation $H_{\mathrm{NW}} \Psi = E \Psi$ can be written as

$$\Psi = \sum_{l=1}^{N} \left(\gamma_{\uparrow,l} a_{\uparrow,l} + \gamma_{\downarrow,l} a_{\downarrow,l} + \eta_{\uparrow,l} b_{\uparrow,l} + \eta_{\downarrow,l} b_{\downarrow,l} \right), \tag{6}$$

with real coefficients $\gamma_{\sigma,l}$ and $\eta_{\sigma,l}$. At $E = 0$, defining the matrices $\boldsymbol{\kappa} = \begin{pmatrix} t & -\alpha \\ \alpha & t \end{pmatrix}$, $\mathbf{u}_l = \begin{pmatrix} \mu_l & \Delta_l - V_x \\ -\Delta_l - V_x & \mu_l \end{pmatrix}$

and the vector of coefficients $\vec{\psi}_l = (\gamma_{\uparrow,l}, \gamma_{\downarrow,l})^T$, the above eigenvalue equation can be written as $0 = \boldsymbol{\kappa}^\dagger \vec{\psi}_{l-1} + \boldsymbol{\kappa} \vec{\psi}_{l+1} + \mathbf{u}_l \vec{\psi}_l$, and from here we obtain the transfer equation

$$\begin{pmatrix} \vec{\psi}_{l+1} \\ \boldsymbol{\kappa}^\dagger \vec{\psi}_l \end{pmatrix} = \mathbf{M}_l \begin{pmatrix} \vec{\psi}_l \\ \boldsymbol{\kappa}^\dagger \vec{\psi}_{l-1} \end{pmatrix}, \tag{7}$$

where

$$\mathbf{M}_l \equiv \begin{pmatrix} -\boldsymbol{\kappa}^{-1} \mathbf{u}_l & -\boldsymbol{\kappa}^{-1} \\ \boldsymbol{\kappa}^\dagger & 0 \end{pmatrix},$$

$$= \begin{pmatrix} \dfrac{-t\mu_l + \alpha \left(V_x - \Delta_l \right)}{t^2 + \alpha^2} & \dfrac{-\alpha\mu_l + t \left(V_x + \Delta_l \right)}{t^2 + \alpha^2} & \dfrac{t}{t^2 + \alpha^2} & \dfrac{\alpha}{t^2 + \alpha^2} \\ \dfrac{\alpha\mu_l + t \left(V_x - \Delta_l \right)}{t^2 + \alpha^2} & \dfrac{-t\mu_l - \alpha \left(V_x + \Delta_l \right)}{t^2 + \alpha^2} & \dfrac{-\alpha}{t^2 + \alpha^2} & \dfrac{t}{t^2 + \alpha^2} \\ -t & -\alpha & 0 & 0 \\ \alpha & -t & 0 & 0 \end{pmatrix} \tag{8}$$

is the lth transfer matrix relating the vectors $\vec{\psi}_{l+1}$ and $\vec{\psi}_{l-1}$. Then, the full transfer matrix of the nanowire, from site $l = 1$ to site $l = N$, is simply given by $\mathbf{M} = \prod_{l=1}^{N} \mathbf{M}_l$. The eigenvalues of $\mathbf{M}$ can be written as $e^{\pm N \lambda_n}$, where λ_n are the (dimensionless) 'Lyapunov exponents' of the system [56], which represent the inverse of the localization length. The connection to localization properties are better understood recalling that the transmission probability from site 1 to site N is $\mathcal{T}_{1N} = \sum_{n=1}^{4} \mathcal{T}_n$, with

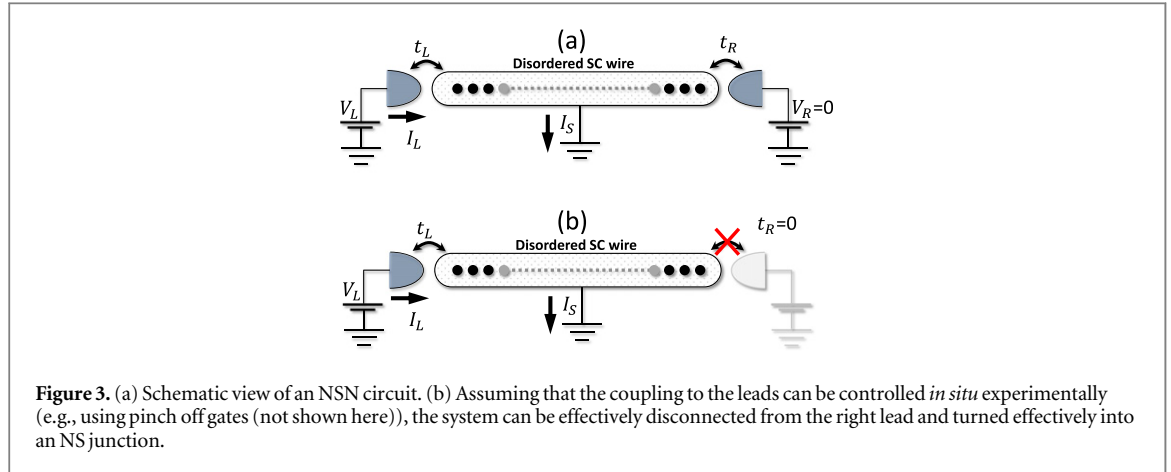$$\mathcal{T}_n = \cosh^{-2} \left(N \lambda_n \right), \tag{9}$$

the transmission eigenvalue corresponding to the nth channel [56].

The connection between the localization and the topological properties of a 'dirty' class D nanowire was made explicit by Akhmerov *et al* [33], who obtained the topological invariant $Q = \mathrm{sign} \left(\prod_{n=1}^{2M} \tanh \lambda_n \right)$, with M the number of channels in the in the the wire. These authors have shown that in the clean case this topological invariant actually reduces to the one derived by Kitaev which is given in terms of the Pfaffian of the Hamiltonian in momentum space [2]. Here we see explicitly that Q changes sign when one of the Lyapunov exponents vanishes and changes sign. This signals the TQPT. As discussed in [27, 33], the TQPT of a class D SC corresponds to a *delocalization point* for zero-energy particles, i.e., one of the Lyapunov exponents λ_n vanishes and changes sign at the TQPT inducing a 'perfect' transmission probability $\mathcal{T}_n = 1$. Everywhere else in the parameter space the system is localized at zero energy, i.e., all λ_n are finite. This crucial result will be addressed in detail in section 6. For the moment, we can check that this idea also works in the clean case: for a clean nanowire, sufficiently close to the TQPT on the topological side, the MBS wavefunctions are localized within the SC correlation length $\xi_{\mathrm{clean}} \simeq \hbar v_F / \Delta (V_x)$, where $\Delta (V_x)$ is the effective SC quasiparticle gap controlled by the Zeeman field. The TQPT is reached at the critical field $V_{x,c} = \sqrt{\Delta_0^2 + \mu_0^2}$, where the quasiparticle gap $\Delta (V_{x,c}) \to 0$ and the localization length $\xi_{\mathrm{clean}} \to \infty$. When $\xi_{\mathrm{clean}} \simeq L_{\mathrm{w}}$, the MBS localized at opposite ends can 'see' each other and overlap forming a Majorana 'channel' that connects the left and the right end. Therefore, for a clean system near the TQPT the smallest Lyapunov exponent is $\lambda_{\mathrm{clean}} \propto \xi_{\mathrm{clean}}^{-1}$. Since the Majorana channel has equal contributions of electrons and holes at $E = 0$, the current sustained by electron-like states exactly cancels the current of hole-like states, and the total electric current vanish. Therefore, the perfectly quantized transmission coefficient $\mathcal{T}_n = 1$ occurring at the TQPT is physically related to the thermal conductance (and not to the electrical conductance). We will return to this point in section 4.

In figure 2(c) we show a 2D color map of the thermal transmission coefficient $\mathcal{T}_{1N}$ for a dirty wire as a function of disorder 'strength' v_μ and applied Zeeman field V_x, fixing all other parameters (chemical potential, pair-potential profile, etc) according to table 1. These parameters correspond exactly to those used in

Table 1. Parameters used in the model (5) in the numerical simulations in figures 2, 4 and 5. The hopping parameter $t = 1$ meV has been chosen to reproduce a ratio $L_w/\xi_{clean} \approx 15$. The average chemical potential μ_0 has been chosen to reproduce the reported experimental value of the critical Zeeman field [9] (i.e, $B \simeq 250$ mT) using the formula [5] $V_{x,c} = \sqrt{\Delta_0^2 + \mu_0^2}$ and assuming weak disorder.

Parameter	Value in InSb (if applicable)	TB equivalent
Wire length	$L_w = 2\ \mu$m	$N = 300$
Mass	$m = 0.015\ m_e$	$m = \left(2ta^2\right)^{-1}$
Chemical Potential	Not known	$\mu_0 = -1.72\ t$
Bulk pairing potential	$\Delta_0 = 250\ \mu$eV	$\Delta_0 = 0.05\ t$
Rashba spin–orbit coupling	$\alpha_R = 0.2$ eV .	$\alpha = \sqrt{m\alpha_R^2 t/2} = 0.15\ t$
Slope of pairing profile	Not applicable	$d_\Delta = 30\ a$

Figure 3. (a) Schematic view of an NSN circuit. (b) Assuming that the coupling to the leads can be controlled *in situ* experimentally (e.g., using pinch off gates (not shown here)), the system can be effectively disconnected from the right lead and turned effectively into an NS junction.

figures 2(a) and (b) for the *same configuration of disorder potential*, and each dot corresponds to each one of the curves in those figures. The blue regions indicate the points for which the transmission coefficient is close to the maximal value $\mathcal{T}_{1N} = 1$, and therefore indicate the approximate location of the TQPT. Therefore, figure 2(c) allows to determine the phase boundary separating the topological from the non-topological region. Note that this boundary has an intrinsic width which scales as $\propto 1/N \propto 1/L_w$. More precisely, as we will see in section 6, the width corresponds to the Thouless energy $\hbar v_F/L_w$. For the parameters in table 1 and in the absence of disorder, we estimate an upper bound $L_w/\xi \simeq 15$, where we have used the estimation for the minimal value of the SC correlation length $\xi_{clean} = \hbar v_F/\Delta_0 \simeq 20\ a$ and $L_w = 300\ a$.

Contrasting figures 2(a)–(c), we note that the four curves on the top correspond to dots in (c) which are closer to the topological phase boundary, where the topological protection is expected to be more fragile. This seems to be in agreement with the fact that figure 2(a) shows a splitting in the ZBP. The ZBP appearing in the corresponding curves in figures 2(b) and the apparent inconsistency with figure 2(a) (i.e., peaks not correlated) will be addressed and discussed in the next section. In contrast, the four central curves in both figures (a) and (b) show a more robust ZBP, which is consistent with the corresponding points in figure 2(c) located further from the boundary. As we see, this analysis showing all curves 'side-to-side' is potentially helpful to interpret the experimental transport results. A natural question arises: is it possible to access the information in (c) *experimentally*? This will be the subject of the next sections.

4. Electronic transport properties in the NSN configuration

We now turn to quantities with more relevance to current experimental measurements. To that end, we introduce a term in the Hamiltonian describing the coupling to external normal leads (see figure 3(a))

$$H_{mix} = \sum_\sigma \left(t_L d_{Lk,\sigma}^\dagger c_{1,\sigma} + t_R d_{Rk,\sigma}^\dagger c_{N,\sigma} \right) + \text{h.c.}, \tag{10}$$

where the term where $t_{L(R)}$ is the coupling to the left (right) lead and $d_{L(R)k,s}^\dagger$ is the corresponding creation operator for fermions with quantum number k and spin σ. The external leads are modeled as large Fermi liquids with Hamiltonian $H_{lead,j} = \sum_{k,\sigma} \epsilon_k d_{j,k,\sigma}^\dagger d_{j,k,\sigma}$, where $j = \{L, R\}$. We assume that each lead is in equilibrium at a chemical potential $\mu_j = eV_j$ controlled by external voltages, and that the SC nanowire is grounded. The expression for the electric current flowing through the contacts is $I_j = e \langle dN_j/dt \rangle = ie \langle [H, N_j] \rangle/\hbar$

$= \mathrm{i}e \langle [H_{\mathrm{mix}}, N_j] \rangle / \hbar$, which can be written using equations of motion in terms of the Green's function in the nanowire [57, 58]. The excess current I_S flowing to ground through the bulk of the SC wire ensures the average conservation of charge $I_L + I_R + I_S = 0$. The conductance matrix of the NSN system equation (1) can be expressed as

$$G_{LL} = \frac{e^2}{h} \int_{-\infty}^{\infty} \mathrm{d}\omega \left[-\frac{\mathrm{d}n_L(\omega)}{\mathrm{d}(eV_L)} \right] \mathrm{Tr} \left[2\mathbf{r}_{eh}^{LL} \left(\mathbf{r}_{eh}^{LL} \right)^{\dagger} + \mathbf{t}_{ee}^{LR} \left(\mathbf{t}_{ee}^{LR} \right)^{\dagger} + \mathbf{t}_{eh}^{LR} \left(\mathbf{t}_{eh}^{LR} \right)^{\dagger} \right]_{\omega}, \tag{11}$$

$$G_{LR} = \frac{e^2}{h} \int_{-\infty}^{\infty} \mathrm{d}\omega \left[\frac{\mathrm{d}n_R(\omega)}{\mathrm{d}(eV_R)} \right] \mathrm{Tr} \left[\mathbf{t}_{ee}^{LR} \left(\mathbf{t}_{ee}^{LR} \right)^{\dagger} - \mathbf{t}_{eh}^{LR} \left(\mathbf{t}_{eh}^{LR} \right)^{\dagger} \right]_{\omega}, \tag{12}$$

$$G_{RL} = \frac{e^2}{h} \int_{-\infty}^{\infty} \mathrm{d}\omega \left[\frac{\mathrm{d}n_L(\omega)}{\mathrm{d}(eV_L)} \right] \mathrm{Tr} \left[\mathbf{t}_{ee}^{RL} \left(\mathbf{t}_{ee}^{RL} \right)^{\dagger} - \mathbf{t}_{eh}^{RL} \left(\mathbf{t}_{eh}^{RL} \right)^{\dagger} \right]_{\omega}, \tag{13}$$

$$G_{RR} = \frac{e^2}{h} \int_{-\infty}^{\infty} \mathrm{d}\omega \left[-\frac{\mathrm{d}n_R(\omega)}{\mathrm{d}(eV_R)} \right] \mathrm{Tr} \left[2\mathbf{r}_{eh}^{RR} \left(\mathbf{r}_{eh}^{RR} \right)^{\dagger} + \mathbf{t}_{ee}^{RL} \left(\mathbf{t}_{ee}^{RL} \right)^{\dagger} + \mathbf{t}_{eh}^{RL} \left(\mathbf{t}_{eh}^{RL} \right)^{\dagger} \right]_{\omega}. \tag{14}$$

These formulas are standard (see [20, 39, 47, 59]) and we do not derive them here. The reader will find more details in the aforementioned references and in appendix. We have defined the normal reflection and transmission matrices (i.e., with subindex '*ee*' or 'electron–electron')

$$\left[\mathbf{r}_{ee}^{LL}(\omega) \right]_{\sigma,\sigma'} = \gamma_L(\omega) g_{1\sigma,1\sigma'}^{r}(\omega),$$

$$\left[\mathbf{r}_{ee}^{RR}(\omega) \right]_{\sigma,\sigma'} = \gamma_R(\omega) g_{N\sigma,N\sigma'}^{r}(\omega),$$

$$\left[\mathbf{t}_{ee}^{LR}(\omega) \right]_{\sigma,\sigma'} = \sqrt{\gamma_L(\omega)\gamma_R(\omega)}\, g_{1\sigma,N\sigma'}^{r}(\omega),$$

and the Andreev reflection and transmission matrices (i.e., with subindex '*eh*' or 'electron–hole')

$$\left[\mathbf{r}_{eh}^{LL}(\omega) \right]_{\sigma,\sigma'} = \gamma_L(\omega) f_{1\sigma,1\sigma'}^{r}(\omega),$$

$$\left[\mathbf{r}_{eh}^{RR}(\omega) \right]_{\sigma,\sigma'} = \gamma_R(\omega) f_{N\sigma,N\sigma'}^{r}(\omega),$$

$$\left[\mathbf{t}_{eh}^{LR}(\omega) \right]_{\sigma,\sigma'} = \sqrt{\gamma_L(\omega)\gamma_R(\omega)}\, f_{1\sigma,N\sigma'}^{r}(\omega),$$

where $g_{ls,ms'}^{r}(\omega)$ and $f_{ls,ms'}^{r}(\omega)$ are the normal and anomalous retarded Green's functions [60] in the nanowire respectively (see appendix). We have also defined the effective couplings to the leads

$$\gamma_j(\omega) = 2\pi t_j^2 \rho_j^0(\omega) \quad (j = L, R), \tag{15}$$

where $\rho_j^0(\omega)$ is the density of states in the *j*-lead. Assuming a large bandwidth in the normal contacts, in the following we set $\rho_j^0(\omega) = \rho_j^0(0)$, the value at the Fermi level.

Let us analyze the physical content of equations (11)–(14). We first focus on the 'local' conductances equations (11) and (14). In these expressions, the first term corresponds to the local contribution $2\mathrm{Tr} \left[\mathbf{r}_{eh}^{LL} \left(\mathbf{r}_{eh}^{LL} \right)^{\dagger} \right]_{\omega}$ and $2\mathrm{Tr} \left[\mathbf{r}_{eh}^{RR} \left(\mathbf{r}_{eh}^{RR} \right)^{\dagger} \right]_{\omega}$, i.e., the Andreev reflection probability at the left and right lead, respectively. These terms are the only terms appearing in the case of NS or SN contacts [18], and they already contain the information about the presence of a MBS localized at the corresponding end. From this perspective, the quantized value of the conductance $2e^2/h$ corresponds to a 'perfect' Andreev reflection $\mathrm{Tr} \left[\mathbf{r}_{eh}^{LL} \left(\mathbf{r}_{eh}^{LL} \right)^{\dagger} \right]_{\omega=0} = 1$ at $T = 0$, due to the presence of the MBS. However, note that in equations (11) and (14) we also encounter a *non-local* contribution $\mathrm{Tr} \left[\mathbf{t}_{ee}^{LR} \left(\mathbf{t}_{ee}^{LR} \right)^{\dagger} + \mathbf{t}_{eh}^{LR} \left(\mathbf{t}_{eh}^{LR} \right)^{\dagger} \right]_{\omega}$, which physically corresponds to particles that travel from one to the other end of the wire, and return to the original lead with information about the opposite lead. These non-local terms are present only in the NSN junctions, and not in the simple NS configuration so far studied extensively in the literature. Our primary motivation for considering NSN junctions (with the 'S' part being the nanowire carrying MBS under suitable conditions) is to study the effect of these non-local terms in the transport experiments, since non-locality is the key concept underlying MBS in the topological phase. Therefore, this contribution must be proportional to the electron–electron and electron–hole *transmission* coefficients, $\mathrm{Tr} \left[\mathbf{t}_{ee}^{LR} \left(\mathbf{t}_{ee}^{LR} \right)^{\dagger} \right]_{\omega}$ and $\mathrm{Tr} \left[\mathbf{t}_{eh}^{LR} \left(\mathbf{t}_{eh}^{LR} \right)^{\dagger} \right]_{\omega}$ respectively, and vanishes if either γ_L or γ_R

vanishes by, e.g., 'pinching off' one of the quantum point contacts using underlying gates (i.e., pinch off gates) (see figure 3(b)). Note that the presence of such a non-local contribution is expected in multi-terminal phase-coherent mesoscopic systems [61].

Interestingly, the thermal conductance G_{th} across the wire [61–63]

$$G_{th} = G_{th,0} \, \text{Tr} \left[\mathbf{t}_{ee}^{LR} \left(\mathbf{t}_{ee}^{LR} \right)^\dagger + \mathbf{t}_{eh}^{LR} \left(\mathbf{t}_{eh}^{LR} \right)^\dagger \right]_\omega , \qquad (16)$$

where $G_{th,0} = \pi^2 k_B^2 T / 6h$ is the thermal quantum of conductance, is closely connected to the non-local contribution in equations (11) and (14), and allows to make a link with our previous discussion in section 3. The connection with the thermal transmission probability $\mathcal{T}_{1N}$ at zero energy is $\mathcal{T}_{1N} = 2 \, \text{Tr} \left[\mathbf{t}_{ee}^{LR} \left(\mathbf{t}_{ee}^{LR} \right)^\dagger + \mathbf{t}_{eh}^{LR} \left(\mathbf{t}_{eh}^{LR} \right)^\dagger \right]_{\omega=0}$. In principle, the information about the TQPT is contained in this expression. However, such thermal measurements are in general very challenging experimentally, and we need to come up with a different approach which is experimentally feasible. In particular, it is desirable to use electrical measurements (i.e., electrical conductance) for observing the non-local MBS correlations at the TQPT and beyond.
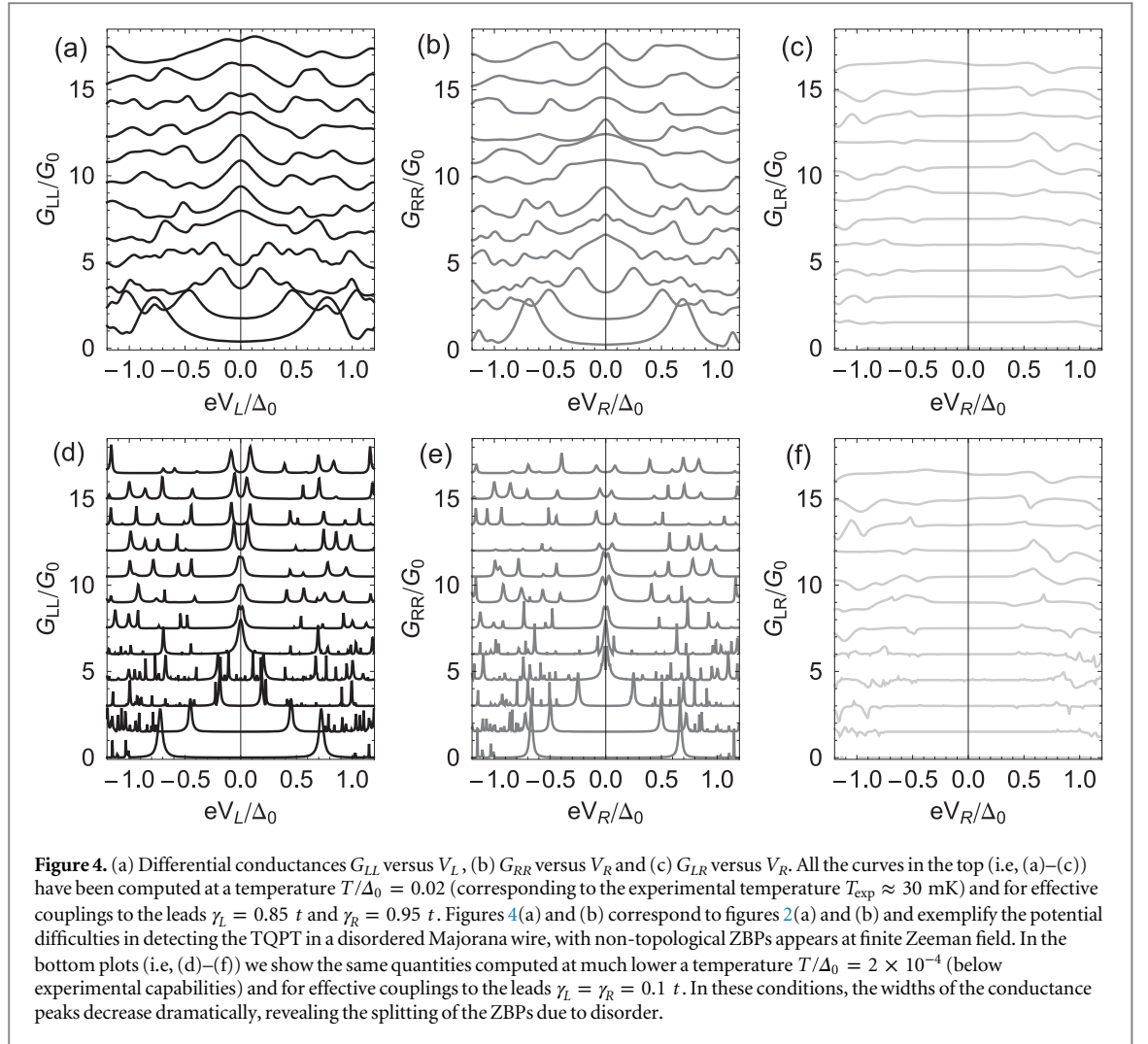
We now briefly discuss equations (12) and (13) (i.e., the so-called *transconductances* G_{LR} and G_{RL}, which obey $G_{RL} = G_{LR}$), where a more explicit difference with respect to the NS geometry appears. Physically, the minus sign in these expressions appears because while electrons contribute with a plus sign to the transport, a hole will contribute a minus sign. As discussed previously in section 3, note that if the system is in the topological phase with end-MBS, particle–hole symmetry dictates that the contributions $\text{Tr} \left[\mathbf{t}_{ee}^{LR} \left(\mathbf{t}_{ee}^{LR} \right)^\dagger \right]_{\omega=0}$ and $\text{Tr} \left[\mathbf{t}_{eh}^{LR} \left(\mathbf{t}_{eh}^{LR} \right)^\dagger \right]_{\omega=0}$ must be identical, and therefore the transconductance must vanish [33]. This might seem to rule out the possibility to see the TQPT via electrical measurements of G_{LR}.

In figures 4(a) and (b) we reproduce the same figures 2(a) and (b), computed for the parameters in table 1, at a temperature $T/\Delta_0 = 0.02$ (which approximately corresponds to the experimental temperature $T_{exp} \approx 60$ mK in [9]), and where we have assumed effective couplings $\gamma_L = 0.85 \, t$ and $\gamma_R = 0.95 \, t$, corresponding to an open wire condition (i.e., 'good' electrical contact with the leads). In figure 4(c) we present a plot for G_{LR} versus V_R for the same parameters. Note that this quantity is rather featureless, and is vanishingly small near zero bias as expected. For comparison, in figures 4(d)–(f) we show G_{LL}, G_{RR} and G_{LR}, respectively, for the same parameters but for a much lower temperature $T/\Delta_0 = 2 \times 10^{-4}$ and smaller couplings $\gamma_L = \gamma_R = 0.1 \, t$. In these conditions the thermal and quasiparticle broadenings decrease dramatically and we realize that the preliminary information about the ZBPs in figures 4(a) and (b) is misleading: the system does not have zero-bias excitations and the peaks are actually split (rather than being a single zero energy peak) in figures 4(d) and (e) at low temperatures and at low transparency of the contacts. This picture is actually consistent with figure 2(c), where the dots corresponding to the largest magnetic fields are very close to the topological phase boundary, and therefore we expect the MBS to recombine into Dirac fermions and consequently the peaks to shift away from zero bias voltage. This allows to interpret the uncorrelated ZBPs for G_{LL} and G_{RR}. The results in figure 4 shows that already for the simple model of equation (5), detection of a 'true' Majorana ZBP based only on the information about the local conductances might be very tricky [23]. Therefore, the presence of ZBPs in the local conductances G_{LL} and G_{RR} cannot by itself be considered as a 'smoking-gun' evidence of the Majorana scenario without some critical considerations of the correlations in the existence of these ZBPs arising from the two end conductances.

5. Electrical detection of topological phase transitions in the NSN configuration

As mentioned before, in the case of clean wires, the TQPT should be observed in the closing and reopening of the gap of electronic excitations in the nanowire. This re-organization of the fermionic spectrum is necessary in order to accommodate a new MBS at zero energy. However, the experiments so far have been unable to report any definitive closing of the gap. It has been suggested that this negative results might originate because while the tunneling occurs at the end of the nanowire, the information about the gap-closing is contained in wavefunctions with most of the weight in the bulk of the nanowire. Therefore, measurements of the LDOS in the middle of the wire [64], capacitive measurements of the total DOS [65], or phase-locked magnetoconductance oscillations in flux-biased topological Josephson junctions [66] should reveal this gap-closing occurring at the TQPT, but no experimental evidence of these predictions have been reported so far in nanowires contacted at the ends.

In addition to characterizing the transport properties of disordered NSN Majorana wires, another goal of the present work is to explore experimental proposals to determine the topological phase diagram. We believe that

Figure 4. (a) Differential conductances G_{LL} versus V_L, (b) G_{RR} versus V_R and (c) G_{LR} versus V_R. All the curves in the top (i.e, (a)–(c)) have been computed at a temperature $T/\Delta_0 = 0.02$ (corresponding to the experimental temperature $T_{exp} \approx 30$ mK) and for effective couplings to the leads $\gamma_L = 0.85\ t$ and $\gamma_R = 0.95\ t$. Figures 4(a) and (b) correspond to figures 2(a) and (b) and exemplify the potential difficulties in detecting the TQPT in a disordered Majorana wire, with non-topological ZBPs appears at finite Zeeman field. In the bottom plots (i.e, (d)–(f)) we show the same quantities computed at much lower a temperature $T/\Delta_0 = 2 \times 10^{-4}$ (below experimental capabilities) and for effective couplings to the leads $\gamma_L = \gamma_R = 0.1\ t$. In these conditions, the widths of the conductance peaks decrease dramatically, revealing the splitting of the ZBPs due to disorder.
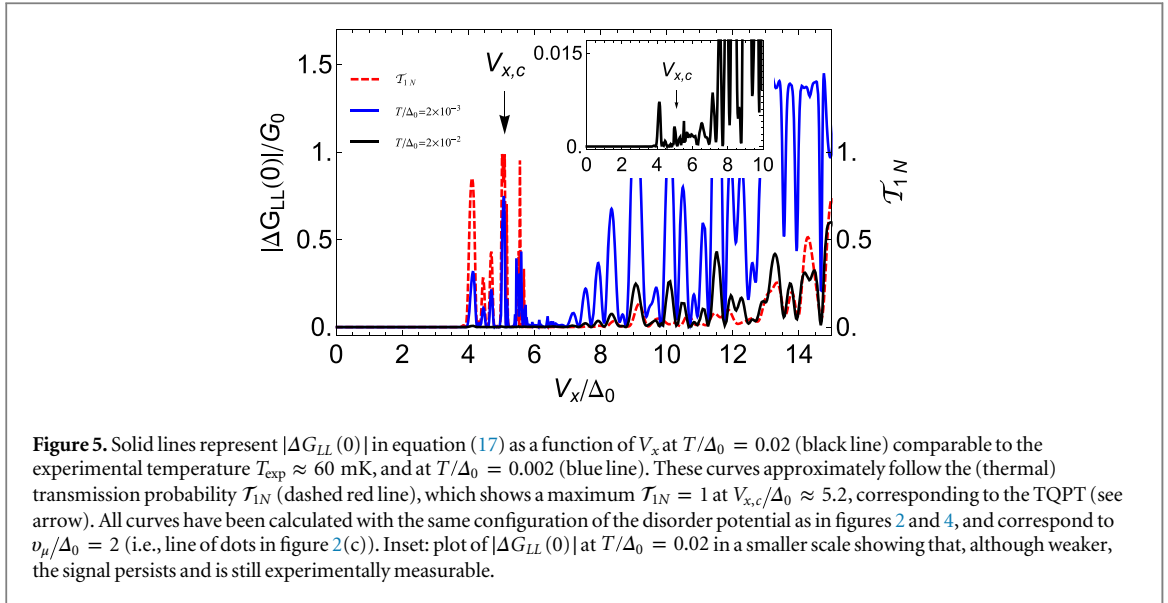
the NSN geometry offers an interesting possibility to achieve this goal, and to provide information about the topological stability of the MBS. In section 3 we stressed that the TQPT in Majorana wires corresponds to a delocalization point at zero energy, a fact that can be detected in the thermal transmission probability across the system. On the other hand, in section 4 we showed that in the NSN geometry, the local conductance of a phase-coherent Majorana nanowire depends on the non-local transmission probability $\text{Tr}\left[\mathbf{t}_{ee}^{LR}\left(\mathbf{t}_{ee}^{LR}\right)^{\dagger} + \mathbf{t}_{eh}^{LR}\left(\mathbf{t}_{eh}^{LR}\right)^{\dagger} \right]_{\omega}$, in addition to the local Andreev reflection coefficient, which exactly corresponds to the (dimensionless) thermal transport at energy ω (see equation (16)). This enables mapping out the topological phase diagram by purely *electrical* measurements [39]. In this section we provide more details in the way the non-local information could be extracted in the NSN configuration in order to obtain the topological phase diagram.

Following [39], we define the following quantity

$$\Delta G_{jj}(0) \equiv G_{jj}(0) - G'_{jj}(0), \tag{17}$$

i.e., the difference of local zero-bias conductances computed for different values of couplings to the *opposite* lead, while keeping all other parameters fixed. The zero-bias conductance at one end $G_{jj}(0)$ is computed for a given value of $\gamma_{\bar{j}}$ (with compact notation $\bar{L} = R$ and $\bar{R} = L$) and $G'_{jj}(0)$ is computed for a different value $\gamma'_{\bar{j}}$. From the experimental point of view, this means using γ_R and γ_L as tuning parameters, something that could be achieved varying the pinch-off gates underneath the ends of the nanowire [9–14]. This constitutes a new experimental knob which has not been explored so far in the Majorana experiment. Note that this quantity (as defined by equation (17)), being a difference, is not quantized and can take either positive or negative values. For this reason in what follows we will take the absolute value.

A priori, it might seem counter-intuitive that the transport through a disordered medium could be influenced by the change of a boundary condition at the far-end. However, this intuition is typically built upon the more usual case of trivial Anderson-localized 1D systems, where any amount of disorder localizes the wavefunctions and therefore any object placed at distances larger than the localization length ξ_{loc} has essentially

Figure 5. Solid lines represent $|\Delta G_{LL}(0)|$ in equation (17) as a function of V_x at $T/\Delta_0 = 0.02$ (black line) comparable to the experimental temperature $T_{exp} \approx 60$ mK, and at $T/\Delta_0 = 0.002$ (blue line). These curves approximately follow the (thermal) transmission probability $\mathcal{T}_{1N}$ (dashed red line), which shows a maximum $\mathcal{T}_{1N} = 1$ at $V_{x,c}/\Delta_0 \approx 5.2$, corresponding to the TQPT (see arrow). All curves have been calculated with the same configuration of the disorder potential as in figures 2 and 4, and correspond to $v_\mu/\Delta_0 = 2$ (i.e., line of dots in figure 2(c)). Inset: plot of $|\Delta G_{LL}|$ at $T/\Delta_0 = 0.02$ in a smaller scale showing that, although weaker, the signal persists and is still experimentally measurable.

no effect. The crucial difference with class D conductors is that $\xi_{loc} \propto \lambda_n^{-1} \to \infty$ at the TQPT (since the gap closes here), i.e., the delocalization point. Therefore, assuming that $L_w < L_\phi$, where L_ϕ is the phase-relaxation length, the aforementioned intuition is usually correct *except* at the TQPT. The physical idea behind using $\Delta G_{jj}(0)$ as an indicator of the TQPT can be seen quite simply in the extreme case when $\gamma'_{\bar{j}} = 0$. In this case, in equations (11) and (14) for G'_{LL} and G'_{RR} respectively, one completely suppresses the coupling to the opposite lead and the transmission coefficients vanish. The remaining part (i.e., Andreev reflection $2\text{Tr}\left[\mathbf{r}_{eh}^{jj}\left(\mathbf{r}_{eh}^{jj}\right)^\dagger\right]_\omega$) is a purely local contribution. Therefore, equation (17) must correspond to a non-local contribution which contains information about the TQPT. This statement is not entirely correct because modifying the coupling $\gamma_{\bar{j}}$ to $\gamma'_{\bar{j}}$ also modifies the local Andreev reflection coefficient through the local anomalous Green's functions $f_{1s,1s'}^r(\omega)$, which contains information about the entire system. Only in the perturbative limit where $\delta\gamma_{\bar{j}} \equiv \gamma'_{\bar{j}} - \gamma_{\bar{j}} \ll \gamma_{\bar{j}}$, one can rigorously show [39] that at the lowest order in $\delta\gamma_{\bar{j}}$, equation (17) becomes

$$\Delta G_{jj}(0) \approx \delta\gamma_{\bar{j}} \frac{e^2}{h} \int_{-\infty}^{\infty} d\omega \left[-\frac{dn_j(\omega)}{d(eV_j)} \right]_{eV_j=0}$$
$$\times \text{Tr}\left[\mathbf{t}_{ee}^{LR}\left(\mathbf{t}_{ee}^{LR}\right)^\dagger + \mathbf{t}_{eh}^{LR}\left(\mathbf{t}_{eh}^{LR}\right)^\dagger \right]_\omega,$$

i.e., proportional to the thermal transmission.

In figure 5 we show $\left|\Delta G_{LL}(0)\right|$ as a function of V_x for the same parameters as before (see table 1), for $v_\mu/\Delta_0 = 2$ and for $\gamma_R = 0.94\ t$ and $\gamma'_R = 0.01\ t$, and $\gamma_L = 0.85\ t$. The black solid line corresponds to the experimental temperature $T_{exp}/\Delta_0 = 0.02$, while the blue solid line corresponds to a temperature $T/\Delta_0 = 2 \times 10^{-3}$ (one order of magnitude smaller). We also show a vertical cut of $\mathcal{T}_{1N}$ (corresponding to $v_\mu/\Delta_0 = 2$ in figure 2(c)) as a red dashed line. That curve indicates the location of the TQPT (i.e., when $\mathcal{T}_{1N} \approx 1$) in a theoretically isolated wire, which occurs at $V_{x,c}/\Delta_0 \approx 5.2$ (indicated by a blue dot in the horizontal axis in figure 5). For $V_x > V_{x,c}$, strictly speaking the system remains in the topologically non-trivial phase, but the strong fluctuations of $\mathcal{T}_{1N}$ indicate a very fragile topological protection of the Majorana modes.

5.1. Experimental considerations

In order to assess the experimental feasibility of our proposal, one important aspect to consider is the effect of a finite temperature. Comparing the black and blue lines in figure 5 we can see that thermal effects dramatically decrease the magnitude of $\Delta G_{jj}(0)$, as can be seen in the overall reduction of the signal when the temperature increases from $T/\Delta_0 = 2 \times 10^{-3}$ to $T/\Delta_0 = 2 \times 10^{-2}$ (comparable to the experimental value $T_{exp} = 60$ mK in [9]). While at higher fields $V_x > V_{x,c}$ the signal is still clearly visible at $T/\Delta_0 = 2 \times 10^{-2}$, closely following the fluctuations in $\mathcal{T}_{1N}$, near the critical field $V_{x,c}$ the signal drops to $\left|\Delta G_{jj}(0)\right| \sim 3 \times 10^{-3} e^2/h$ (see inset in figure 5). Although this value is still experimentally measurable, it would be desirable to minimize thermal effects in order to have a stronger signal to detect the TQPT.

In what follows we show that the effect can still be measured under reasonable experimental conditions. An important point which should be taken into account to minimize thermal effect is that our proposal is expected to work best for short wires, where the maximal ratio L_w/ξ is not too large (in figure 5, using the parameters in table 1, we estimate an upper bound $L_w/\xi \approx 15$). Therefore, using shorter nanowires should yield more robust signals, albeit at the cost of less resolution. This is because the visibility of the electrical signal crucially depends on the width $\hbar v_F/L_w$ of the peak in $\left| \Delta G_{LL}(0) \right|$ (see last paragraph in section 6 for an intuitive explanation). Therefore, a very narrow peak $\hbar v_F/L_w \ll T$ might be hard to detect, or could be washed away by thermal effects or other dissipative mechanisms not considered here. Lower base temperatures or larger induced gaps should also produce a stronger signal, as can be seen in figure 5 (blue line). None of these requirements represent an intrinsic experimental limitation in future samples or experiments. For instance, base temperatures of the order of $T_{exp} \approx 20$ mK have been recently reported in [45], which would produce $T/\Delta_0 \sim 7 \times 10^{-3}$, allowing a stronger signal and better resolution of the transition near the critical field.

We also note that the magnetic fields required to see the signal are also within experimental reach. For the nanowires studied in [9], the large $g \approx 50$ factor produces $V_x/B \approx 1.5$ meV T^{-1}. Assuming a maximal magnetic field of $B_{max} \sim 2$ T (see for instance figure S2 in the supplementary material in that reference) the Zeeman energy can be made as large as $V_x \approx 3$ meV. Recalling that the experimentally induced gap is estimated in $\Delta_0 \approx 0.25$ meV, we conclude that $V_{x,max}/\Delta_0 \sim 12$, which implies that the range of energies in figure 5 is perfectly feasible. We stress that an important requirement for this proposal is that the nanowire must be shorter than the phase-relaxation length $L_w < L_\phi$ for the two end-MBS to hybridize coherently, a condition that is typically very well met in mesoscopic samples.

Overall, from the above discussion we conclude that $\left| \Delta G_{jj}(0) \right|$ is a bona fide indicator of the TQPT and the topological stability of the MBS at low enough temperatures. While the experimental details will obviously depend on non-universal quantities (such as the size of the SC gap, length of the wire, degree of disorder, etc), our results in figure 5 indicate that the nonlocal conductance effect is definitely an experimentally observable quantity at finite temperatures. From a general point of view, our proposed experiment is much easier than either braiding or fractional Josephson effect (although harder perhaps than the straight ZBCP measurement).

Finally, although we have suggested using the pinch off gates as a physical way to effectively tune the coupling to the normal contacts, this is not necessarily the only way to change the parameter γ_{jj}. For instance, schemes using quantum dots (QDs) between the normal contact and the Majorana nanowire [67–69] (i.e., N-QD-S-QD-N setups) will also serve the same purpose. In this case, it would be relatively easy to modify the transparency of the coupling to the lead by changing the gate voltages in each QD. However, the QDs should be large enough to avoid strong Coulomb effects, which might introduce unwanted effects (e.g., Kondo effect [70]) complicating the experimental interpretation. We also mention that in [33], an alternative method to detect the TQPT based on the measurement of the current shot noise was proposed, which would be a complementary to the idea discussed here.

6. Intuitive theoretical picture

In this section we provide a simple theoretical framework to interpret our numerical simulations in previous sections. To that end we focus on a simplified version of the Hamiltonian H_{NW} in equations (2) and (3), which will allow us to obtain an exact solution, therefore providing a valuable physical insight, while retaining at the same time the relevant physics. These simplifications will not modify our main conclusions because they do not depend on the details of H_{NW} itself, but on its *symmetry class* (i.e., class D in this case) which is a robust feature. Therefore, for the present purposes we assume a uniform chemical potential $\mu_0 = \delta\mu(x) = 0$. In this simplified model, disorder enters only through the inhomogeneous pair potential $\Delta(x)$, which we now assume to be generic and not necessarily of the form (4).

It is simpler to start the analysis from the uniform case with periodic boundary conditions, where the band theory helps to visualize the relevant physics related to the TQPT occurring near the point $k = 0$, at the intersection of the spin–orbit coupled bands with different spin projection (see figure 6). The modes at finite momentum $\pm k_F$ are assumed to be gapped by the SC paring interaction (not shown in the picture), and decouple from the relevant sector at $k = 0$. Projecting the original fermionic operator around this point and linearizing the bands results in a helical liquid model described by the Hamiltonian [24]

$$H_{NW} = \int dx \left[-i\hbar v_F \left(\psi_R^\dagger \partial_x \psi_R - \psi_L^\dagger \partial_x \psi_L \right) \right.$$
$$\left. + \Delta(x) \left(\psi_L \psi_R + \text{h.c.} \right) + \left(V_x \psi_R^\dagger \psi_L + \text{h.c.} \right) \right], \tag{18}$$
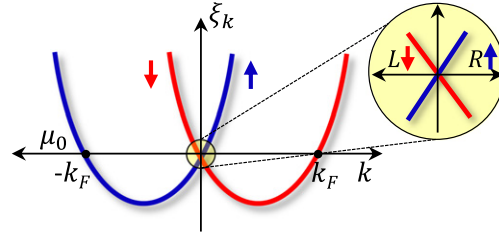
Figure 6. Dispersion relation of a nanowire with Rashba spin–orbit coupling, in the absence of proximity-induced pairing $\Delta(x) = 0$, in the absence of Zeeman field $V_x = 0$ and for $\mu_0 = \delta\mu(x) = 0$. Under these conditions, chosen to simplify the theoretical model in equation (18), a helical liquid arises near the point $k = 0$.

where $\psi_R \simeq \psi_\uparrow(x)$ and $\psi_L \simeq \psi_\downarrow(x)$ result from spin-momentum locking around $k = 0$ due to the spin–orbit interaction. We now introduce the Majorana basis

$$\boldsymbol{\eta}_1(x) = \begin{pmatrix} \eta_{1,R} \\ \eta_{1,L} \end{pmatrix} \equiv \frac{1}{\sqrt{2}} \begin{pmatrix} -\psi_R - \psi_R^\dagger \\ \mathrm{i}\psi_L - \mathrm{i}\psi_L^\dagger \end{pmatrix}, \tag{19}$$

$$\boldsymbol{\eta}_2(x) = \begin{pmatrix} \eta_{2,R} \\ \eta_{2,L} \end{pmatrix} \equiv \frac{1}{\sqrt{2}} \begin{pmatrix} \mathrm{i}\psi_R - \mathrm{i}\psi_R^\dagger \\ \psi_L + \psi_L^\dagger \end{pmatrix}, \tag{20}$$

in terms of which (18) splits into two independent modes

$$H_{\mathrm{NW}} = \frac{1}{2} \sum_{n=1,2} \int \mathrm{d}x \; \boldsymbol{\eta}_n^T(x) \Big\{ -\mathrm{i}\hbar v_F \hat{\tau}_z \partial_x$$
$$- \Big[V_x + (-1)^n \Delta(x) \Big] \hat{\tau}_y \Big\} \boldsymbol{\eta}_n(x), \tag{21}$$

where we have introduced the Pauli matrices $\hat{\tau}_i$ acting on *LR* space. The emergence of Majorana zero-modes can be easily seen by solving the eigenvalue equation for $E = 0$

$$\Big\{ -\mathrm{i}\hbar v_F \hat{\tau}_z \partial_x - \Big[V_x + (-1)^n \Delta(x) \Big] \hat{\tau}_y \Big\} \boldsymbol{\eta}_n(x) = 0, \tag{22}$$

whose solution is

$$\boldsymbol{\eta}_n(x) = \exp \Big\{ \frac{1}{\hbar v_F} \int_0^x \mathrm{d}x' \Big[V_x + (-1)^n \Delta\big(x'\big) \Big] \hat{\tau}_x \Big\} \boldsymbol{\eta}_n(0). \tag{23}$$

We now define the zero-energy eigenmodes

$$\boldsymbol{\chi}_n^\pm(x) = \exp \Big\{ \pm \frac{1}{\hbar v_F} \int_0^x \mathrm{d}x' \Big[V_x + (-1)^n \Delta\big(x'\big) \Big] \Big\} \begin{pmatrix} 1 \\ \pm 1 \end{pmatrix}, \tag{24}$$

in terms of which the expression for a generic MBS localized at the origin (i.e., the left end of the wire) is

$$\boldsymbol{\eta}(x) = a_1 \boldsymbol{\chi}_1(x) + a_2 \boldsymbol{\chi}_2(x). \tag{25}$$

Although the form of the eigenmodes (24) is more convenient for our purposes, we mention here that one can easily bring this expression into the more familiar form of the Jackiw–Rebbi soliton solution [71] applying a rotation along the $\hat{y}$−axis $\hat{R} = \mathrm{e}^{\mathrm{i}\frac{\pi}{4}\hat{\tau}_y}$, which transforms to the usual eigenvectors of the operator $\hat{\tau}_z$. In order to ensure the existence of MBS we need to find normalizable solutions that decrease sufficiently fast as $x \to \infty$ and that satisfy generic boundary conditions. For a wire of length L_w, we can define the quantity

$$\lambda_n = \frac{1}{L_w \hbar v_F} \int_0^{L_w} \mathrm{d}x' \Big[V_x + (-1)^n \Delta\big(x'\big) \Big], \tag{26}$$

which in the limit $L_w \to \infty$ corresponds to the Lyapunov exponent of the system at zero energy for the channel n. In terms of these quantities, note that there are two possible situations [2]:

(i) Both λ_1 and λ_2 have the same sign, in which case we need to choose either $\boldsymbol{\eta}(x) = a_1 \boldsymbol{\chi}_1^+(x) + a_2 \boldsymbol{\chi}_2^+(x)$ or $\boldsymbol{\eta}(x) = a_1 \boldsymbol{\chi}_1^-(x) + a_2 \boldsymbol{\chi}_2^-(x)$ in equation (25), the sign depending on which of the modes decays for $x > 0$. Since there are two decaying contributions allowed, we can satisfy generic boundary conditions at the origin. For instance, if the system is a trivial insulator for $x < 0$, then the boundary condition
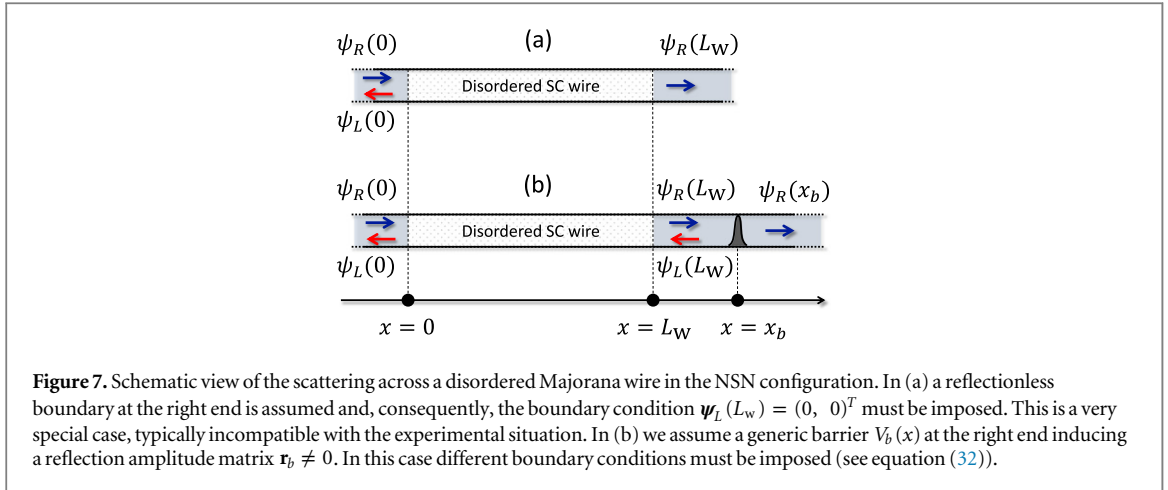
Figure 7. Schematic view of the scattering across a disordered Majorana wire in the NSN configuration. In (a) a reflectionless boundary at the right end is assumed and, consequently, the boundary condition $\psi_L(L_w) = (0,\ 0)^T$ must be imposed. This is a very special case, typically incompatible with the experimental situation. In (b) we assume a generic barrier $V_b(x)$ at the right end inducing a reflection amplitude matrix $\mathbf{r}_b \neq 0$. In this case different boundary conditions must be imposed (see equation (32)).

$\boldsymbol{\eta}(0) = (0,\ 0)^T$ must be imposed. This is verified with $a_1 + a_2 = 0$. Other boundary conditions for open wires will be analyzed later.

(ii) The Lyapunov exponents λ_1 and λ_2 have different signs. Then equation (25) is a linear combination of spinors $\boldsymbol{\chi}^+$ and $\boldsymbol{\chi}^-$. This makes it impossible to satisfy generic boundary conditions, except for accidental situations which are not protected against local perturbations. For instance, in our previous example of a vanishing boundary condition at the origin, the condition $\boldsymbol{\eta}(0) = (0,\ 0)^T$ implies that $a_1 + a_2 = a_1 - a_2 = 0$, which can only be satisfied for $a_1 = a_2 = 0$. Therefore the MBS does not exist.

From this analysis, we conclude that the TQPT occurs when one of the Lyapunov exponents λ_n passes through zero and changes sign, making explicit the connection between the localization properties of a D-class nanowire and its topological properties. This is a robust feature which is independent of the details of the microscopic Hamiltonian as it depends only on the symmetry classification. Assuming that the magnetic field V_x is such that $\lambda_2 > 0$, the condition for the topological phase reduces to

$$\lambda_1 = \frac{1}{\hbar v_F}\left[V_x - \bar{\Delta}\right] > 0, \tag{27}$$

where we have defined the average gap $\bar{\Delta} \equiv \frac{1}{L_w}\int_0^{L_w} dx'\, \Delta(x')$. Note that this expression coincides with the expression derived by Sau *et al* $V_x > \sqrt{\mu_0^2 + \Delta_0^2}$ for the ideal system, i.e., for a uniform $\Delta(x) \to \Delta_0$ and for $\mu_0 = 0$ [5].

6.1. Open wires

We now assume that our wire is connected to conducting leads at both ends, and focus on the transport across the NSN configuration at zero energy, as depicted in figure 7(a). We define the scattering matrix [33]

$$\begin{pmatrix} \boldsymbol{\psi}_R(L_w) \\ \boldsymbol{\psi}_L(0) \end{pmatrix} = \mathcal{S}_0 \begin{pmatrix} \boldsymbol{\psi}_R(0) \\ \boldsymbol{\psi}_L(L_w) \end{pmatrix}, \qquad \mathcal{S}_0 = \begin{pmatrix} \mathbf{t}_0 & \mathbf{r}'_0 \\ \mathbf{r}_0 & \mathbf{t}'_0 \end{pmatrix}, \tag{28}$$

where $\boldsymbol{\psi}_\nu(x) \equiv \left(\eta_{1,\nu}(x),\ \eta_{2,\nu}(x)\right)^T$ are ν-moving (with $\nu = \{L, R\}$) scattering Majorana states in the left and right leads ($x = 0$ and $x = L_w$, respectively). In the Majorana basis, $\mathcal{S}_0$ is a real orthonormal matrix $\mathcal{S}_0^T = \mathcal{S}_0^\dagger = \mathcal{S}_0^{-1}$ [33]. Since from equation (18), the modes $n = \{1, 2\}$ are decoupled and independent, the transmission and reflection matrices, $\mathbf{t}_0$, $\mathbf{t}'_0$ and $\mathbf{r}_0$, $\mathbf{r}'_0$ respectively, acquire a diagonal form, an can be diagonalized independently with diagonal elements $t_{0,n}$, $t'_{0,n}$ and $r_{0,n}$, $r'_{0,n}$. Without loss of generality, in what follows we assume that the only incident modes are right-moving modes arriving from the left lead. This imposes the boundary conditions (see figure 7(a))

$$\boldsymbol{\psi}_L(L_w) = \begin{pmatrix} 0 \\ 0 \end{pmatrix}, \qquad \boldsymbol{\psi}_R(0) = \begin{pmatrix} 1 \\ 1 \end{pmatrix}, \tag{29}$$

which in combination with equations (23) and (28), allow to obtain closed analytical expressions for the reflection and transmission coefficients

$$t_{0,n} = \cosh^{-1}\left(L_w \lambda_n\right), \tag{30}$$

$$r_{0,n} = -\tanh\left(L_{\mathrm{w}}\lambda_n\right),\tag{31}$$

and we recover equation (9) for the transmission probability.

Exactly at the TQPT, the determinant of the reflection matrix vanishes and a 'Majorana channel' with perfect transmission opens at zero energy. As mentioned in section 3, Akhmerov *et al* [33]. derived a suitable topological invariant for a dirty class D nanowire directly in terms of the reflection matrix as $Q = \mathrm{sign}\,\mathrm{Det}\,\mathbf{r}_0 = \mathrm{sign}\,\mathrm{Det}$ $\mathbf{r}_0' = \prod_n \tanh\lambda_{0,n}$, and suggested that the TQPT could be observed as a quantized peak in the thermal conductance through the nanowire $G_{\mathrm{th}}/G_0 = \mathrm{Tr}\left(\mathbf{t}_0\mathbf{t}_0^\dagger\right) = \sum_n \cosh^{-2}\left(L_{\mathrm{w}}\lambda_n\right)$, where we recover the result in section 3. This is consistent with the results in [27], where the authors predicted that the transition from topologically trivial to topologically non-trivial phases should be a *delocalization* transition, and at both sides of this point the system should be generically localized at zero energy. However, unfortunately a Majorana channel is necessarily neutral (i.e., particles and holes have equal weight in the MBS wavefunction) and therefore cannot support an electrical current. On the other hand, direct thermal transport measurements could provide evidence of the transition [33], but this remains an experimental challenge.

To understand better our experimental proposal in section 5 we first note that the form of equations (30) and (31) are a consequence of the particular 'reflectionless' boundary conditions (29) at the right end. In other words, in figure 7(a) at the right end of the wire, the barrier at $x = L_{\mathrm{w}}$ is 'transparent', and all right-moving Majorana states $\psi_R\left(L_{\mathrm{w}}\right)$ that are transmitted to the right-end of the nanowire disappears in the right lead. As shown in [39], this is not the most general situation. The generic presence of a barrier $V_b(x)$ at the end of the nanowire induces some probability of reflection, and imposes a non-vanishing amplitude $\psi_L\left(L_{\mathrm{w}}\right)$ (see figure 7(b)). More physically, any potential profile at the end nanowire, or the presence of pinch off gates could play the role of a barrier inducing a non-ideal coupling to the right-lead. For simplicity, let us consider a point-like scatterer sitting at some point $x_b > L_{\mathrm{w}}$, as depicted in figure 7(b). The crucial point is that, in the presence of this new barrier, the reflectionless boundary conditions (29) are no longer possible. Assuming that the potential barrier $V_b(x)$ induces reflection and transmission amplitudes, $r_{b,n}$ and $t_{b,n}$ respectively (subject to the unitary condition $|r_{b,n}|^2 + |t_{b,n}|^2 = 1$), the scattering matrix obeys

$$\begin{pmatrix}\psi_R(x_b)\\\psi_L(L_{\mathrm{w}})\end{pmatrix} = \mathcal{S}_b\begin{pmatrix}\psi_R(L_{\mathrm{w}})\\\psi_L(x_b)\end{pmatrix},\qquad \mathcal{S}_b = \begin{pmatrix}\mathbf{t}_b & \mathbf{r}_b'\\\mathbf{r}_b & \mathbf{t}_b'\end{pmatrix},\tag{32}$$

and the new boundary conditions for right-moving Majorana states arriving from the left lead are

$$\psi_L(x_b) = \begin{pmatrix}0\\0\end{pmatrix},\qquad \psi_R(0) = \begin{pmatrix}1\\1\end{pmatrix}.\tag{33}$$

In combination with equations (28) and (32), we obtain the transmission and reflection amplitudes at the left-end of the *complete* system (nanowire *and* barrier):

$$t_n = \frac{t_{b,n}t_{0,n}}{1 - r_{b,n}r_{0,n}},\tag{34}$$

$$r_n = r_{0,n} + t_{0,n}\left(\frac{r_{b,n}}{1 - r_{b,n}r_{0,n}}\right)t_{0,n}.\tag{35}$$

In particular, the last term in equation (35) physically represents processes in which the right-moving Majorana mode is transmitted to the right-end of the nanowire with amplitude $t_{0,n}$ and is reflected back as a left-mover with amplitude $r_{b,n}$. The denominator in $r_{b,n}(1 - r_{b,n}r_{0,n})^{-1} = r_{b,n} + r_{b,n}r_{0,n}r_{b,n} + \cdots$, represents an infinite sum of all backward and forward internal reflection processes occurring in the wire. Importantly, even though r_n is a local quantity involving the reflection at the left-end of the nanowire, equation (35) explicitly contains non-local contributions involving scattering at the right-end, and its form is closely related to equations (11) and (14) for the local differential conductances. This is a milestone result in phase-coherent mesoscopic transport which has been well-known for almost thirty years [61].

The above considerations summarize the main theoretical ideas in this work. Assuming that $r_{b,n}$ is a parameter that can be modified *in situ* in the experiment (as is the case of the pinch off gates in [9]), equation (35) shows that a small variation $\delta r_{b,n}$ gives rise to a modification $\delta r_n \propto \cosh^{-2}\left(L_{\mathrm{w}}\lambda_n\right)\delta r_{b,n}$, which would be non-vanishing precisely at the TQPT and which could be detected in *electrical* measurements. This is the main idea of our proposal, and the main reason for us to propose experiments in the NSN geometry in order to establish the existence of the TQPT and the MBS in Majorana nanowires.

7. Summary and conclusions

We have explored the transport properties of disordered Majorana nanowires in the NSN configuration with the nanowire being the superconducting S part and the two N parts are ordinary metallic tunneling contacts with suitable gates controlling their tunnel barriers. This type of geometry is being explored at present by experimental groups studying Majorana bound states, and consequently, our study might be of relevance for the interpretation of these results. The NSN configuration allows to access qualitatively new information about the topological properties of the system through a direct study of non-local correlations inherent in the MBS which cannot be done in the NS geometry mostly used in the experimental Majorana measurements so far. Physically, this is possible because in the NSN configuration one can test the *bulk* properties, in addition to the boundary properties which are the only properties accessible in NS contacts. In our work we have adopted a comprehensive point of view, which links the deep theoretical aspects (i.e., topological invariants, topological classification, TQPT and topological phase diagram) with the experimental observables (i.e., tunneling transport). We have also proposed a useful tool, i.e., the difference of local conductances equation (17), to detect the TQPT occurring as a function of the applied Zeeman field and to assess the topological protection of a given system experimentally. The experimental signal equation (17) is expected to be stronger and more robust to thermal broadening effects for 'short' wires with ratio $L_{\rm w}/\xi$ not too large ($L_{\rm w}/\xi \approx 15$ in this work) and $L_{\rm w} < L_\phi$, i.e., smaller than the phase-relaxation length. We stress that this proposal to detect the TQPT is qualitatively different from the study of non-local correlations in the shot noise measurements [48–51]. Despite the simplifications assumed in this work, we note that our main ideas do not rely on the details of our model, but on generic symmetry properties of class D Bogoliubov–de Gennes Hamiltonians. In particular, the fact that the TQPT correspond to a delocalized point at zero energy is a robust feature in these non-interacting Hamiltonians. In the presence of interactions the theoretical description of transport becomes much harder and remains an open issue. However, we speculate that the main idea behind equation (17) should remain valid in that case too. Interestingly, using the framework of Abelian bosonization, in [32] it was shown that the low-temperature properties of a disordered class D wire with repulsive short-range electron–electron interactions (i.e., dimensionless Luttinger parameter [72] $K < 1$) are adiabatically connected to those of a non-interacting wire (i.e., with $K = 1$), provided the system remains in the topological phase as the interaction is adiabatically 'turned on'. In particular, the delocalized nature of the TQPT in the interacting case can be inferred using an instanton calculation in the presence of disorder, where the equivalent of the localization length (i.e., the exponent of the instanton action) diverges at the critical point [32].

Acknowledgments

Appendix. Derivation of equations (11)–(14)

Starting from equations (5) and (10), the expression for the electric current flowing through the contacts is $I_j = e \langle {\rm d}N_j / {\rm d}t \rangle = {\rm i}e \langle [H, N_j] \rangle / \hbar = {\rm i}e \langle [H_{\rm mix}, N_j] \rangle / \hbar$, which can be written in terms of the Green's function at the contacts [57, 58]

$$I_L = \frac{{\rm i}e}{\hbar} \sum_\sigma t_L \left[\left\langle d_{L,\sigma}^\dagger c_{1,\sigma} \right\rangle - \left\langle c_{1,\sigma}^\dagger d_{L,\sigma} \right\rangle \right], \tag{A.1}$$

$$I_R = \frac{{\rm i}e}{\hbar} \sum_\sigma t_R \left[\left\langle d_{R,\sigma}^\dagger c_{N,\sigma} \right\rangle - \left\langle c_{N,\sigma}^\dagger d_{R,\sigma} \right\rangle \right], \tag{A.2}$$

where we have defined $d_{j,\sigma} = \frac{1}{\sqrt{\mathcal{N}_j}} \sum_k d_{jk,\sigma}$, with $j = \{L, R\}$, and where $\mathcal{N}_j$ is the number of sites in the lead j.

With these definitions, note that the currents are positive if particles move into the leads (i.e., exit the SC), and negative otherwise. On the other hand, charge conservation demands that $I_L + I_R + I_S = 0$, where I_S is the excess current that flows to ground through the SC (see figure 3). Within the Baym–Kadanoff–Keldysh formalism [73, 74] we define the lesser and bigger Green's functions

$$g_{i\sigma,j\sigma'}^<(t) \equiv {\rm i}e \left\langle c_{i,\sigma}^\dagger c_{j,\sigma}(t) \right\rangle, \tag{A.3}$$

$$g_{i\sigma,j\sigma'}^>(t) \equiv -{\rm i}e \left\langle c_{i,\sigma}(t) c_{j,\sigma}^\dagger \right\rangle, \tag{A.4}$$

so that we can write the currents as

$$I_L = \frac{e}{\hbar} t_L \sum_\sigma \int_{-\infty}^\infty \frac{d\omega}{2\pi} \left[g^<_{L\sigma,1\sigma}(\omega) - g^<_{1\sigma,L\sigma}(\omega) \right], \tag{A.5}$$

$$I_R = \frac{e}{\hbar} t_R \sum_\sigma \int_{-\infty}^\infty \frac{d\omega}{2\pi} \left[g^<_{R\sigma,N\sigma}(\omega) - g^<_{N\sigma,R\sigma}(\omega) \right]. \tag{A.6}$$

Using equations of motion, we can express equations (A.5) and (A.6) in terms of local Green's functions as [57, 58]

$$I_L = -\frac{e}{h} t_L^2 \sum_\sigma \int_{-\infty}^\infty d\omega \left[g^{0,<}_{L\sigma,L\sigma}(\omega) g^>_{1\sigma,1\sigma}(\omega) - g^{0,>}_{L\sigma,L\sigma}(\omega) g^<_{1\sigma,1\sigma}(\omega) \right], \tag{A.7}$$

$$I_R = -\frac{e}{h} t_R^2 \sum_\sigma \int_{-\infty}^\infty d\omega \left[g^{0,<}_{R\sigma,R\sigma}(\omega) g^>_{N\sigma,N\sigma}(\omega) - g^{0,>}_{R\sigma,R\sigma}(\omega) g^<_{N\sigma,N\sigma}(\omega) \right]. \tag{A.8}$$

The unperturbed Green's functions $g^{0,\gtrless}_{j\sigma,j\sigma}(\omega)$ in the leads

$$g^{0,<}_{j\sigma,j\sigma}(\omega) = 2\pi i \rho^0_{j,\sigma}(\omega) n_j(\omega), \tag{A.9}$$

$$g^{0,>}_{j\sigma,j\sigma}(\omega) = 2\pi i \rho^0_{j,\sigma}(\omega) \left[n_j(\omega) - 1 \right], \tag{A.10}$$

contain the information about the Fermi distribution functions $n_j(\omega) = n_F(\omega + \mu_j)$ at the leads. Substituting equations (A.9) and (A.10) into equations (A.7) and (A.8) yields

$$I_L = -\frac{ie}{h} 2\pi t_L^2 \sum_\sigma \int_{-\infty}^\infty d\omega \, \rho^0_{L,\sigma}(\omega) \left\{ n_L(\omega) \left[g^r_{1\sigma,1\sigma}(\omega) - g^a_{1\sigma,1\sigma}(\omega) \right] + g^<_{1\sigma,1\sigma}(\omega) \right\}, \tag{A.11}$$

$$I_R = -\frac{ie}{h} 2\pi t_R^2 \sum_\sigma \int_{-\infty}^\infty d\omega \, \rho^0_{R,\sigma}(\omega) \left\{ n_R(\omega) \left[g^r_{N\sigma,N\sigma}(\omega) - g^a_{N\sigma,N\sigma}(\omega) \right] + g^<_{N\sigma,N\sigma}(\omega) \right\}, \tag{A.12}$$

where we have used the identity $g^>(\omega) - g^<(\omega) = g^r(\omega) - g^a(\omega)$ [73, 74]. Obtaining an explicit expression for the currents I_L and I_R in the general case is quite cumbersome. However, since we will be interested only in the conductance, we note that there is a great simplification if we compute directly the conductance matrix by deriving the currents with respect to the voltages V_L, V_R. Then

$$G_{LL} \equiv \frac{dI_L}{dV_L} = -\frac{ie^2}{h} 2\pi t_L^2 \sum_\sigma \int_{-\infty}^\infty d\omega \, \rho^0_{L,\sigma}(\omega)$$
$$\times \left\{ \frac{dn_L(\omega)}{d(eV_L)} \left[g^r_{1\sigma,1\sigma}(\omega) - g^a_{1\sigma,1\sigma}(\omega) \right] + \frac{dg^<_{1\sigma,1\sigma}(\omega)}{d(eV_L)} \right\}, \tag{A.13}$$

$$G_{LR} \equiv \frac{dI_L}{dV_R} = -\frac{ie^2}{h} 2\pi t_L^2 \sum_\sigma \int_{-\infty}^\infty d\omega \, \rho^0_{L,\sigma}(\omega) \frac{dg^<_{1\sigma,1\sigma}(\omega)}{d(eV_R)}, \tag{A.14}$$

$$G_{RL} \equiv \frac{dI_R}{dV_L} = -\frac{ie^2}{h} 2\pi t_R^2 \sum_\sigma \int_{-\infty}^\infty d\omega \, \rho^0_{R,\sigma}(\omega) \frac{dg^<_{N\sigma,N\sigma}(\omega)}{d(eV_L)}, \tag{A.15}$$

$$G_{RR} \equiv \frac{dI_R}{dV_R} = -\frac{ie^2}{h} 2\pi t_R^2 \sum_\sigma \int_{-\infty}^\infty d\omega \, \rho^0_{R,\sigma}(\omega)$$
$$\times \left\{ \frac{dn_R(\omega)}{d(eV_R)} \left[g^r_{N\sigma,N\sigma}(\omega) - g^a_{N\sigma,N\sigma}(\omega) \right] + \frac{dg^<_{N\sigma,N\sigma}(\omega)}{d(eV_R)} \right\}. \tag{A.16}$$

Therefore, we see that the problem is reduced to finding the Green's functions in the superconducting system. In a non-interacting system, the full Green's function verifies the Dyson's equation in Nambu space [57]

$$\mathcal{G}^{\gtrless}(\omega) = \left[1 + \mathcal{G}^r(\omega) \left(\mathcal{T}_L + \mathcal{T}_R \right) \right] \mathcal{G}^{0,\gtrless}(\omega) \left[1 + \left(\mathcal{T}_L + \mathcal{T}_R \right) \mathcal{G}^a(\omega) \right], \tag{A.17}$$

$$\mathcal{G}^{(r,a)}(\omega) = \mathcal{G}^{0,(r,a)}(\omega) + \mathcal{G}^{0,(r,a)}(\omega) \left(\mathcal{T}_L + \mathcal{T}_R \right) \mathcal{G}^{(r,a)}(\omega), \tag{A.18}$$

where we have introduced the Nambu notation

$$
\mathcal{G}^{\nu}_{i\sigma,j\sigma'}(z) = \begin{pmatrix} g^{\nu}_{i\sigma,j\sigma'}(z) & f^{\nu}_{i\sigma,j\sigma'}(z) \\ \bar{f}^{\nu}_{i\sigma,j\sigma'}(z) & \bar{g}^{\nu}_{i\sigma,j\sigma'}(z) \end{pmatrix},
\tag{A.19}
$$

with $\nu = \{>, <, r, a\}$, and where

$$
\mathcal{T}_j = \begin{pmatrix} t_j & 0 \\ 0 & -t_j \end{pmatrix}.
\tag{A.20}
$$

The unperturbed Keldysh Green's functions (i.e., computed for $t_L = t_R = 0$) are

$$
\mathcal{G}^{0,<}_{i\sigma,j\sigma'}(\omega) = 2\pi i \rho^{0}_{i\sigma,j\sigma'}(\omega) n_F(\omega),
\tag{A.21}
$$

$$
\mathcal{G}^{0,>}_{i\sigma,j\sigma'}(\omega) = 2\pi i \rho^{0}_{i\sigma,j\sigma'}(\omega)\big[n_F(\omega) - 1 \big],
\tag{A.22}
$$

$$
\rho^{0}_{i\sigma,j\sigma'}(\omega) = -\frac{1}{\pi} \operatorname{Im}\big[\mathcal{G}^{0,r}_{i\sigma,j\sigma'}(\omega) \big] = \begin{pmatrix} \rho^{0}_{i\sigma,j\sigma'}(\omega) & \zeta^{0}_{i\sigma,j\sigma'}(\omega) \\ \zeta^{0}_{i\sigma,j\sigma'}(\omega) & \bar{\rho}^{0}_{i\sigma,j\sigma'}(\omega) \end{pmatrix}.
\tag{A.23}
$$

We only need the derivative with respect to the voltages, which are only in the leads. Therefore

$$
\frac{dg^{\gtrless}_{1\sigma,1\sigma}}{d(eV_L)} = 2\pi i t_L^2 \sum_s \left[\frac{dn_L}{d(eV_L)} \rho_L^0 g^r_{1\sigma,1s} g^a_{1s,1\sigma} + \frac{d\bar{n}_L}{d(eV_L)} \bar{\rho}_L^0 f^r_{1\sigma,1s} \bar{f}^a_{1s,1\sigma} \right],
$$

$$
\frac{dg^{\gtrless}_{1\sigma,1\sigma}}{d(eV_R)} = 2\pi i t_R^2 \sum_s \left[\frac{dn_R}{d(eV_R)} \rho_R^0 g^r_{1\sigma,Ns} g^a_{Ns,1\sigma} + \frac{d\bar{n}_R}{d(eV_R)} \bar{\rho}_R^0 f^r_{1\sigma,Ns} \bar{f}^a_{Ns,1\sigma} \right],
$$

$$
\frac{dg^{\gtrless}_{N\sigma,N\sigma}}{d(eV_L)} = 2\pi i t_L^2 \sum_s \left[\frac{dn_L}{d(eV_L)} \rho_L^0 g^r_{N\sigma,1s} g^a_{1s,N\sigma} + \frac{d\bar{n}_L}{d(eV_L)} \bar{\rho}_L^0 f^r_{N\sigma,1s} \bar{f}^a_{1s,N\sigma} \right],
$$

$$
\frac{dg^{\gtrless}_{N\sigma,N\sigma}}{d(eV_R)} = 2\pi i t_R^2 \sum_s \left[\frac{dn_R}{d(eV_R)} \rho_R^0 g^r_{N\sigma,Ns} g^a_{Ns,N\sigma} + \frac{d\bar{n}_R}{d(eV_R)} \bar{\rho}_R^0 f^r_{N\sigma,Ns} \bar{f}^a_{Ns,N\sigma} \right].
$$

Replacing these expressions into equations (A.13)–(A.16), and using the result $g^r_{j\sigma,j\sigma}(\omega) - g^a_{j\sigma,j\sigma}(\omega) = -2\pi i \rho_{j\sigma}(\omega)$, where we have defined the local density of states $\rho_{j\sigma}(\omega) \equiv \rho_{j\sigma,j\sigma}(\omega)$, yields

$$
G_{LL} = -\frac{e^2}{h} \sum_\sigma \int_{-\infty}^{\infty} d\omega \, \gamma_L(\omega) \left[\frac{dn_L}{d(eV_L)} 2\pi \rho_{1\sigma} - \sum_s \frac{dn_L}{d(eV_L)} \gamma_L g^r_{1\sigma,1s} g^a_{1s,1\sigma} \right.
$$
$$
\left. - \sum_s \frac{d\bar{n}_L}{d(eV_L)} \bar{\gamma}_L f^r_{1\sigma,1s} \bar{f}^a_{1s,1\sigma} \right]_\omega,
\tag{A.24}
$$

$$
G_{LR} = \frac{e^2}{h} \sum_{\sigma,s} \int_{-\infty}^{\infty} d\omega \left[\gamma_L \gamma_R \frac{dn_R}{d(eV_R)} g^r_{1\sigma,Ns} g^a_{Ns,1\sigma} + \frac{d\bar{n}_R}{d(eV_R)} \gamma_L \bar{\gamma}_R f^r_{1\sigma,Ns} \bar{f}^a_{Ns,1\sigma} \right]_\omega,
\tag{A.25}
$$

$$
G_{RL} = \frac{e^2}{h} \sum_{\sigma,s} \int_{-\infty}^{\infty} d\omega \left[\frac{dn_L}{d(eV_L)} \gamma_R \gamma_L g^r_{N\sigma,1s} g^a_{1s,N\sigma} + \frac{d\bar{n}_L}{d(eV_L)} \gamma_R \bar{\gamma}_L f^r_{N\sigma,1s} \bar{f}^a_{1s,N\sigma} \right]_\omega,
\tag{A.26}
$$

$$
G_{RR} = -\frac{e^2}{h} \sum_\sigma \int_{-\infty}^{\infty} d\omega \, \gamma_R(\omega) \left[\frac{dn_R}{d(eV_R)} 2\pi \rho_{N\sigma} - \sum_s \frac{dn_R}{d(eV_R)} \gamma_R g^r_{N\sigma,Ns} g^a_{Ns,N\sigma} \right.
$$
$$
\left. - \sum_s \frac{d\bar{n}_R}{d(eV_R)} \bar{\gamma}_R f^r_{N\sigma,Ns} \bar{f}^a_{Ns,N\sigma} \right]_\omega,
\tag{A.27}
$$

where we have defined the broadening

$$
\gamma_j(\omega) = 2\pi t_j^2 \rho_j^0(\omega),
\tag{A.28}
$$

$$\bar{\gamma}_j(\omega) = 2\pi t_j^2 \bar{\rho}_j^0(\omega). \tag{A.29}$$

To make contact with BTK theory [59, 75], we can express these results in a more standard form by recalling that $M_L(\omega) = 2\pi \operatorname{Tr}\left[\boldsymbol{\Gamma}_L(\omega)\boldsymbol{\rho}_1(\omega)\right] = \sum_\sigma 2\pi\gamma_L(\omega)\rho_{1\sigma}(\omega)$ is the number of modes in the lead L at frequency ω, and $M_R(\omega) = 2\pi \operatorname{Tr}\left[\boldsymbol{\Gamma}_R(\omega)\boldsymbol{\rho}_N(\omega)\right] = \sum_\sigma 2\pi\gamma_R(\omega)\rho_{N\sigma}(\omega)$ is the analog quantity for lead R, where we have defined the matrices $\boldsymbol{\Gamma}_{L(R)}(\omega) = \begin{pmatrix} \gamma_{L(R)}(\omega) & 0 \\ 0 & \gamma_{L(R)}(\omega) \end{pmatrix}$, and $\boldsymbol{\rho}_{1(N)}(\omega) = 2\pi\begin{pmatrix} \rho_{L(N),\uparrow}(\omega) & 0 \\ 0 & \rho_{L(N),\downarrow}(\omega) \end{pmatrix}$ (see [76]). On the other hand, defining the matrices

$$\mathbf{r}_{ee}^{LL}(\omega) = \begin{pmatrix} \gamma_L g_{1\uparrow,1\uparrow}^r & \gamma_L g_{1\uparrow,1\downarrow}^r \\ \gamma_L g_{1\downarrow,1\uparrow}^r & \gamma_L g_{1\downarrow,1\downarrow}^r \end{pmatrix}_\omega,$$

$$\mathbf{r}_{eh}^{LL}(\omega) = \begin{pmatrix} \gamma_L f_{1\uparrow,1\uparrow}^r & \gamma_L f_{1\uparrow,1\downarrow}^r \\ \gamma_L f_{1\downarrow,1\uparrow}^r & \gamma_L f_{1\downarrow,1\downarrow}^r \end{pmatrix}_\omega,$$

$$\mathbf{r}_{ee}^{RR}(\omega) = \begin{pmatrix} \gamma_R g_{N\uparrow,N\uparrow}^r & \gamma_R g_{N\uparrow,N\downarrow}^r \\ \gamma_R g_{N\downarrow,N\uparrow}^r & \gamma_R g_{N\downarrow,N\downarrow}^r \end{pmatrix}_\omega,$$

$$\mathbf{r}_{eh}^{RR}(\omega) = \begin{pmatrix} \gamma_R f_{N\uparrow,N\uparrow}^r & \gamma_R f_{N\uparrow,N\downarrow}^r \\ \gamma_R f_{N\downarrow,N\uparrow}^r & \gamma_R f_{N\downarrow,N\downarrow}^r \end{pmatrix}_\omega,$$

$$\mathbf{t}_{ee}^{LR}(\omega) = \begin{pmatrix} \sqrt{\gamma_L\gamma_R} g_{1\uparrow,N\uparrow}^r & \sqrt{\gamma_L\gamma_R} g_{1\uparrow,N\downarrow}^r \\ \sqrt{\gamma_L\gamma_R} g_{N\downarrow,N\uparrow}^r & \sqrt{\gamma_L\gamma_R} g_{1\downarrow,N\downarrow}^r \end{pmatrix}_\omega,$$

$$\mathbf{t}_{eh}^{LR}(\omega) = \begin{pmatrix} \sqrt{\gamma_L\gamma_R} f_{1\uparrow,N\uparrow}^r & \sqrt{\gamma_L\gamma_R} f_{1\uparrow,N\downarrow}^r \\ \sqrt{\gamma_L\gamma_R} f_{N\downarrow,N\uparrow}^r & \sqrt{\gamma_L\gamma_R} f_{1\downarrow,N\downarrow}^r \end{pmatrix}_\omega,$$

we can express our equations (A.24)–(A.27) in the BTK language as [59, 75]

$$G_{LL} = \frac{e^2}{h} \int_{-\infty}^{\infty} d\omega \left\{ -\frac{dn_L}{d(eV_L)} M_L + \frac{dn_L}{d(eV_L)} \operatorname{Tr}\left[\mathbf{r}_{ee}^{LL}\left(\mathbf{r}_{ee}^{LL}\right)^\dagger\right] + \frac{d\bar{n}_L}{d(eV_L)} \operatorname{Tr}\left[\mathbf{r}_{eh}^{LL}\left(\mathbf{r}_{eh}^{LL}\right)^\dagger\right] \right\}_\omega, \tag{A.30}$$

$$G_{LR} = \frac{e^2}{h} \int_{-\infty}^{\infty} d\omega \left\{ \frac{dn_R}{d(eV_R)} \operatorname{Tr}\left[\mathbf{t}_{ee}^{LR}\left(\mathbf{t}_{ee}^{LR}\right)^\dagger\right] + \frac{d\bar{n}_R}{d(eV_R)} \operatorname{Tr}\left[\mathbf{t}_{eh}^{LR}\left(\mathbf{t}_{eh}^{LR}\right)^\dagger\right] \right\}_\omega, \tag{A.31}$$

$$G_{RL} = \frac{e^2}{h} \int_{-\infty}^{\infty} d\omega \left\{ \frac{dn_L}{d(eV_L)} \operatorname{Tr}\left[\mathbf{t}_{ee}^{RL}\left(\mathbf{t}_{ee}^{RL}\right)^\dagger\right] + \frac{d\bar{n}_L}{d(eV_L)} \operatorname{Tr}\left[\mathbf{t}_{eh}^{RL}\left(\mathbf{t}_{eh}^{RL}\right)^\dagger\right] \right\}_\omega, \tag{A.32}$$

$$G_{RR} = \frac{e^2}{h} \int_{-\infty}^{\infty} d\omega \left\{ -\frac{dn_R}{d(eV_R)} M_R + \frac{dn_R}{d(eV_R)} \operatorname{Tr}\left[\mathbf{r}_{ee}^{RR}\left(\mathbf{r}_{ee}^{RR}\right)^\dagger\right] + \frac{d\bar{n}_R}{d(eV_R)} \operatorname{Tr}\left[\mathbf{r}_{eh}^{RR}\left(\mathbf{r}_{eh}^{RR}\right)^\dagger\right] \right\}_\omega, \tag{A.33}$$

where for convenience we have omitted the argument ω inside the brackets.

In order to make explicit the non-local terms in these expressions we make use of the identity [76]

$$\boldsymbol{\mathcal{G}}^r(\omega) - \boldsymbol{\mathcal{G}}^a(\omega) = \boldsymbol{\mathcal{G}}^r(\omega)\left[\boldsymbol{\Sigma}^r(\omega) - \boldsymbol{\Sigma}^a(\omega)\right]\boldsymbol{\mathcal{G}}^a(\omega), \tag{A.34}$$

From here, the following results are obtained

$$g_{1\sigma,1\sigma}^r(\omega) - g_{1\sigma,1\sigma}^a(\omega) = -2\pi i \rho_{1,\sigma}(\omega) = -2\pi i \sum_s \left[t_L^2 \rho_L^0 g_{1\sigma,1s}^r g_{1s,1\sigma}^a \right.$$

$$\left. + t_L^2 \bar{\rho}_L^0 f_{1\sigma,1s}^r \bar{f}_{1s,1\sigma}^a + t_R^2 \rho_R^0 g_{1\sigma,Ns}^r g_{Ns,1\sigma}^a + t_R^2 \bar{\rho}_R^0 f_{1\sigma,Ns}^r \bar{f}_{Ns,1\sigma}^a \right], \tag{A.35}$$

$$g_{N\sigma,N\sigma}^r(\omega) - g_{N\sigma,N\sigma}^a(\omega) = -2\pi i \rho_{N,\sigma}(\omega) = -2\pi i \sum_s \left[t_R^2 \rho_R^0 g_{N\sigma,Ns}^r g_{Ns,N\sigma}^a \right.$$

$$\left. + t_R^2 \bar{\rho}_R^0 f_{N\sigma,Ns}^r \bar{f}_{Ns,N\sigma}^a + t_L^2 \rho_L^0 g_{N\sigma,1s}^r g_{1s,N\sigma}^a + t_L^2 \bar{\rho}_L^0 f_{N\sigma,1s}^r \bar{f}_{1s,N\sigma}^a \right], \tag{A.36}$$

and hence, substituting into equations (A.30)–(A.33), we obtain

$$G_{LL} = \frac{e^2}{h} \int_{-\infty}^{\infty} d\omega \left[-\frac{dn_L(\omega)}{d(eV_L)} \right] \left\{ 2 \operatorname{Tr}\left[\mathbf{r}_{eh}^{LL}\left(\mathbf{r}_{eh}^{LL}\right)^{\dagger} \right] + \operatorname{Tr}\left[\mathbf{t}_{ee}^{LR}\left(\mathbf{t}_{ee}^{LR}\right)^{\dagger} \right] + \operatorname{Tr}\left[\mathbf{t}_{eh}^{LR}\left(\mathbf{t}_{eh}^{LR}\right)^{\dagger} \right] \right\}_{\omega}, \quad (A.37)$$

$$G_{LR} = \frac{e^2}{h} \int_{-\infty}^{\infty} d\omega \left[\frac{dn_R(\omega)}{d(eV_R)} \right] \left\{ \operatorname{Tr}\left[\mathbf{t}_{ee}^{LR}\left(\mathbf{t}_{ee}^{LR}\right)^{\dagger} \right] - \operatorname{Tr}\left[\mathbf{t}_{eh}^{LR}\left(\mathbf{t}_{eh}^{LR}\right)^{\dagger} \right] \right\}_{\omega}, \quad (A.38)$$

$$G_{RL} = \frac{e^2}{h} \int_{-\infty}^{\infty} d\omega \left[\frac{dn_L(\omega)}{d(eV_L)} \right] \left\{ \operatorname{Tr}\left[\mathbf{t}_{ee}^{RL}\left(\mathbf{t}_{ee}^{RL}\right)^{\dagger} \right] - \operatorname{Tr}\left[\mathbf{t}_{eh}^{RL}\left(\mathbf{t}_{eh}^{RL}\right)^{\dagger} \right] \right\}_{\omega}, \quad (A.39)$$

$$G_{RR} = \frac{e^2}{h} \int_{-\infty}^{\infty} d\omega \left[-\frac{dn_R(\omega)}{d(eV_R)} \right] \left\{ 2 \operatorname{Tr}\left[\mathbf{r}_{eh}^{RR}\left(\mathbf{r}_{eh}^{RR}\right)^{\dagger} \right] + \operatorname{Tr}\left[\mathbf{t}_{ee}^{RL}\left(\mathbf{t}_{ee}^{RL}\right)^{\dagger} \right] + \operatorname{Tr}\left[\mathbf{t}_{eh}^{RL}\left(\mathbf{t}_{eh}^{RL}\right)^{\dagger} \right] \right\}_{\omega}, \quad (A.40)$$

which correspond to equations (11)–(14).

References

[1] Read N and Green D 2000 *Phys. Rev. B* **61** 10267–97
[2] Kitaev A Y 2001 Unpaired Majorana fermions in quantum wires *Phys.—Usp.* **44** 131
[3] Nayak C, Simon S H, Stern A, Freedman M and Das Sarma S 2008 Non-Abelian anyons and topological quantum computation *Rev. Mod. Phys.* **80** 1083
[4] Fu L and Kane C L 2008 Superconducting proximity effect and Majorana fermions at the surface of a topological insulator *Phys. Rev. Lett.* **100** 096407
[5] Sau J D, Lutchyn R M, Tewari S and das Sarma S 2010 *Phys. Rev. Lett* **104** 040502
[6] Lutchyn R M, Sau J D and Das Sarma S 2010 Majorana fermions and a topological phase transition in semiconductor–superconductor heterostructures *Phys. Rev. Lett.* **105** 077001
[7] Oreg Y, Refael G and von Oppen F 2010 Helical liquids and Majorana bound states in quantum wires *Phys. Rev. Lett.* **105** 177002
[8] Sau J D, Tewari S, Lutchyn R M, Stanescu T D and Das Sarma S 2010 *Phys. Rev. B* **82** 214509
[9] Mourik V, Zuo K, Frolov S M, Plissard S R, Bakkers E P A M and Kouwenhoven L P 2012 *Science* **336** 1003
[10] Das A, Ronen Y, Most Y, Oreg Y, Heiblum M and Shtrikman H 2012 Evidence of Majorana fermions in an Al—InAs nanowire topological superconductor *Nat. Phys.* **8** 887
[11] Deng M T, Yu C L, Huang G Y, Larsson M, Caroff P and Xu H Q 2012 Anomalous zero-bias conductance peak in a nbinsb nanowire nb hybrid device *Nano Lett.* **12** 6414–9
[12] Rokhinson L P, Liu X and Furdyna J K 2012 The fractional a.c. Josephson effect in a semiconductor–superconductor nanowire as a signature of Majorana particles *Nat. Phys.* **8** 795
[13] Finck A D K, van Harlingen D J, Mohseni P K, Jung K and Li X 2013 Anomalous modulation of a zero-bias peak in a hybrid nanowire-superconductor device *Phys. Rev. Lett.* **110** 126406
[14] Churchill H O H, Fatemi V, Grove-Rasmussen K, Deng M T, Caroff P, Xu H Q and Marcus C M 2013 Superconductor-nanowire devices from tunneling to the multichannel regime: zero-bias oscillations and magnetoconductance crossover *Phys. Rev. B* **87** 241401
[15] Nadj-Perge S, Drozdov I K, Bernevig B A and Yazdani A 2013 Proposal for realizing Majorana fermions in chains of magnetic atoms on a superconductor *Phys. Rev.* **88** 020407
[16] Jiang L, Kitagawa T, Alicea J, Akhmerov A R, Pekker D, Refael G, Ignacio Cirac J, Demler E, Lukin M D and Zoller P 2011 Majorana fermions in equilibrium and in driven cold-atom quantum wires *Phys. Rev. Lett.* **106** 220402
[17] Sengupta K, Zutic I, Kwon H-J, Yakovenko V M and Das Sarma S 2001 Midgap edge states and pairing symmetry of quasi-one-dimensional organic superconductors *Phys. Rev. B* **63** 144531
[18] Law K T, Lee P A and Ng T K 2009 Majorana fermion induced resonant Andreev reflection *Phys. Rev. Lett.* **103** 237001
[19] Flensberg K 2010 Tunneling characteristics of a chain of Majorana bound states *Phys. Rev. B* **82** 180516
[20] Prada E, San-Jose P and Aguado R 2012 Transport spectroscopy of *NS* nanowire junctions with Majorana fermions *Phys. Rev. B* **86** 180503
[21] Roy D, Bolech C J and Shah N 2012 *Phys. Rev. B* **86** 094503
[22] Pikulin D I, Dahlhaus J P, Wimmer M, Schomerus H and Beenakker C W J 2012 *New J. Phys.* **14** 125011
[23] Liu J, Potter A C, Law K T and Lee P A 2012 Zero-bias peaks in the tunneling conductance of spin–orbit-coupled superconducting wires with and without Majorana end-states *Phys. Rev. Lett.* **109** 267002
[24] Bagrets D and Altland A 2012 Class *D* spectral peak in Majorana quantum wires *Phys. Rev. Lett.* **109** 227005
[25] Kells G, Meidan D and Brouwer P W 2012 Near-zero-energy end states in topologically trivial spin–orbit coupled superconducting nanowires with a smooth confinement *Phys. Rev. B* **86** 100503
[26] Rieder M-T, Kells G, Duckheim M, Meidan D and Brouwer P W 2012 Endstates in multichannel spinless *p*-wave superconducting wires *Phys. Rev. B* **86** 125423
[27] Motrunich O, Damle K and Huse D A 2001 Griffiths effects and quantum critical points in dirty superconductors without spin-rotation invariance: one-dimensional examples *Phys. Rev. B* **63** 224204
[28] Brouwer P W, Furusaki A, Gruzberg I A and Mudry C 2000 *Phys. Rev. Lett.* **85** 1064
[29] Gruzberg I A, Read N and Vishveshwara S 2005 Localization in disordered superconducting wires with broken spin-rotation symmetry *Phys. Rev. B* **71** 245124
[30] Brouwer P W, Duckheim M, Romito A and von Oppen F 2011a Probability distribution of Majorana end-state energies in disordered wires *Phys. Rev. Lett.* **107** 196804
[31] Brouwer P W, Duckheim M, Romito A and von Oppen F 2011b Topological superconducting phases in disordered quantum wires with strong spin–orbit coupling *Phys. Rev. B* **84** 144526

[32] Lobos A M, Lutchyn R M and Das Sarma S 2012 *Phys. Rev. Lett.* **109** 146403

[33] Akhmerov A R, Dahlhaus J P, Hassler F, Wimmer M and Beenakker C W J 2011 Quantized conductance at the Majorana phase transition in a disordered superconducting wire *Phys. Rev. Lett.* **106** 057001

[34] DeGottardi W, Sen D and Vishveshwara S 2011 Topological phases, Majorana modes and quench dynamics in a spin ladder system *New J. Phys.* **13** 065028

[35] DeGottardi W, Sen D and Vishveshwara S 2013 Majorana fermions in superconducting 1D systems having periodic, quasiperiodic, and disordered potentials *Phys. Rev. Lett.* **110** 146404

[36] Sau J D, Tewari S and Das Sarma S 2012 Experimental and materials considerations for the topological superconducting state in electron- and hole-doped semiconductors: searching for non-Abelian Majorana modes in 1D nanowires and 2D heterostructures *Phys. Rev. B* **85** 064512

[37] Lin C-H, Sau J D and Das Sarma S 2012 Zero-bias conductance peak in Majorana wires made of semiconductor/superconductor hybrid structures *Phys. Rev. B* **86** 224511

[38] Adagideli İ, Wimmer M and Teker A 2014 Effects of electron scattering on the topological properties of nanowires: Majorana fermions from disorder and superlattices *Phys. Rev. B* **89** 144506

[39] Fregoso B M, Lobos A M and Das Sarma S 2013 Electrical detection of topological quantum phase transitions in disordered Majorana nanowires *Phys. Rev. B* **88** 180507

[40] Sau J D and Das Sarma S 2013 Density of states of disordered topological superconductor–semiconductor hybrid nanowires *Phys. Rev. B* **88** 064506

[41] Rainis D, Trifunovic L, Klinovaja J and Loss D 2013 Towards a realistic transport modeling in a superconducting nanowire with Majorana fermions *Phys. Rev. B* **87** 024515

[42] Hui H-Y, Sau J D and Das Sarma S 2014 Generalized Eilenberger theory for Majorana zero-mode-carrying disordered *p*-wave superconductors *Phys. Rev. B* **90** 064516

[43] Takei S, Fregoso B M, Hui H-Y, Lobos A M and Das Sarma S 2013 Soft superconducting gap in semiconductor Majorana nanowires *Phys. Rev. Lett.* **110** 186803

[44] Ziino N L B, Krogstrup P, Madsen M H, Johnson E, Wagner J B, Marcus C M, Nygård J and Jespersen T S 2013 Epitaxial aluminum contacts to InAs nanowires (arXiv:1309.4569)

[45] Chang W, Albrecht S M, Jespersen T S, Kuemmeth F, Krogstrup P J, Nygård J and Marcus C M 2015 Hard gap in epitaxial semiconductor–superconductor nanowires *Nat. Nanotechnology* **10** 232

[46] Stanescu T D, Lutchyn R M and Das Sarma S 2014 Soft superconducting gap in semiconductor-based Majorana nanowires *Phys. Rev. B* **90** 085302

[47] Blonder G E, Tinkham M and Klapwijk T M 1982 Transition from metallic to tunneling regimes in superconducting microconstrictions: excess current, charge imbalance, and supercurrent conversion *Phys. Rev. B* **25** 4515

[48] Bolech C J and Demler E 2007 Observing Majorana bound states in *p*-wave superconductors using noise measurements in tunneling experiments *Phys. Rev. Lett.* **98** 237002

[49] Nilsson J, Akhmerov A R and Beenakker C W J 2008 Splitting of a cooper pair by a pair of Majorana bound states *Phys. Rev. Lett.* **101** 120403

[50] Liu J, Zhang F-C and Law K T 2013 Majorana fermion induced nonlocal current correlations in spin–orbit coupled superconducting wires *Phys. Rev. B* **88** 064509

[51] Zocher B and Rosenow B 2013 Modulation of Majorana-induced current cross-correlations by quantum dots *Phys. Rev. Lett.* **111** 036802

[52] Stanescu T D, Lutchyn R M and Das Sarma S 2011 *Phys. Rev. B* **84** 144522

[53] Lutchyn R M, Stanescu T D and Das Sarma S 2011 Search for Majorana fermions in multiband semiconducting nanowires *Phys. Rev. Lett.* **106** 127001

[54] Black-Schaffer A M 2011 Self-consistent superconducting proximity effect at the quantum spin hall edge *Phys. Rev. B* **83** 060504

[55] Vercruyssen N, Verhagen T G A, Flokstra M G, Pekola J P and Klapwijk T M 2012 Evanescent states and nonequilibrium in driven superconducting nanowires *Phys. Rev. B* **85** 224503

[56] Beenakker C W J 1997 Random-matrix theory of quantum transport *Rev. Mod. Phys.* **69** 731

[57] Cuevas J C, Martín-Rodero A and Yeyati A L 1996 *Phys. Rev.* **54** 7366–79

[58] Meir Y and Wingreen N S 1992 *Phys. Rev. Lett.* **68** 2512

[59] Anantram M P and Datta S 1996 *Phys. Rev. B* **53** 16390–402

[60] Fetter A L and Walecka J D 1971 *Quantum Theory of Many-Particle Systems* (New York: McGraw-Hill)

[61] Büttiker M 1986 Four-terminal phase-coherent conductance *Phys. Rev. Lett.* **57** 1761–4

[62] Landauer R 1957 *IBM J. Res. Dev.* **1** 233

[63] Büttiker M, Imry Y, Landauer R and Pinhas S 1985 Generalized many-channel conductance formula with application to small rings *Phys. Rev. B* **31** 6207–15

[64] Stanescu T D, Tewari S, Sau J D and Das Sarma S 2012 To close or not to close: the fate of the superconducting gap across the topological quantum phase transition in Majorana-carrying semiconductor nanowires *Phys. Rev. Lett.* **109** 266402

[65] Appelbaum I 2013 *Appl. Rev. Lett.* **103** 122604

[66] Diez M, Fulga I C, Pikulin D I, Wimmer M, Akhmerov A R and Beenakker C W J 2013 *Phys. Rev. B* **87** 125406

[67] Leijnse M and Flensberg K 2012 Parity qubits and poor man's Majorana bound states in double quantum dots *Phys. Rev. B* **86** 134528

[68] Wang P, Cao Y, Gong M, Xiong G and Li X-Q 2013 *Europhys. Lett.* **103** 57016

[69] Vernek E, Penteado P H, Seridonio A C and Egues J C 2014 Subtle leakage of a Majorana mode into a quantum dot *Phys. Rev. B* **89** 165314

[70] Hewson A C 1993 *The Kondo Problem to Heavy Fermions* (Cambridge: Cambridge University Press)

[71] Jackiw R and Rebbi C 1976 Solitons with fermion number 1/2 *Phys. Rev. D* **13** 3398–409

[72] Giamarchi T 2004 *Quantum Physics in One Dimension* (Oxford: Oxford University Press)

[73] Kadanoff L P and Baym G 1989 *Quantum Statistical Mechanics* (Cambridge, MA: Perseus Books)

[74] Mahan G D 1981 *Many Particle Physics* (New York: Plenum)

[75] Blonder G E, Tinkham M and Klapwijk T M 1982 Transition from metallic to tunneling regimes in superconducting microconstrictions: excess current, charge imbalance, and supercurrent conversion *Phys. Rev. B* **25** 4515

[76] Datta S 1995 *Electronic Transport in Mesoscopic Systems* (Cambridge: Cambridge University Press)